PHYSICAL REVIEW D **79,** 023522 (2009)

Bouncing braneworld cosmologies and initial conditions to inflation

R. Maier and I. Damião Soares

Centro Brasileiro de Pesquisas Físicas, Rua Dr. Xavier Sigaud 150, Urca Rio de Janeiro. CEP 22290-180-RJ, Brazil

E. V. Tonini

Centro Federal de Educação Tecnológica do Espírito Santo, Avenida Vitória, 1729, Jucutuquara, Vitória CEP 29040-780-ES, Brazil

(Received 3 November 2008; published 29 January 2009)

We examine the full nonlinear dynamics of closed Friedmann-Robertson-Walker universes in the framework of *D*-branes formalism. Friedmann equations contain additional terms arising from the bulk-brane interaction that provide a concrete model for nonsingular bounces in the early phase of the Universe. We construct nonsingular cosmological scenarios sourced with perfect fluids and a massive inflaton field, which are past eternal, oscillatory, and may emerge into an inflationary phase due to nonlinear resonance mechanisms. Oscillatory behavior becomes metastable when the system is driven into a resonance window of the parameter space of the models, with consequent breakup of KAM tori that trap the inflaton, leading the Universe to the inflationary regime. A construction of the resonance chart of the models is made. Resonance windows are labeled by an integer $n \geq 2$, where n is related to the ratio of the frequencies in the scale factor/scalar field degrees of freedom. They are typically small compared to the volume of the whole parameter space, and we examine the constraints imposed by nonlinear resonance in the physical domain of initial configurations so that inflation may be realized. We discuss the complex dynamics arising in this preinflationary stage, the structural stability of the resonance pattern and some of its possible imprints in the physics of inflation. We also approach the issue of initial configurations that are connected to a chaotic exit to inflation. Pure scalar field bouncing cosmologies are constructed. Contrary to models with perfect fluid components, the structure of the bouncing dynamics is highly sensitive to the initial amplitude and to the mass of the inflaton; dynamical potential barriers allowing for bounces appear as a new feature of the dynamics. We argue that if our actual Universe is a brane inflated by a parametric resonance mechanism triggered by the inflaton, some observable cosmological parameters should then have a signature of the particular resonance from which the brane inflated.

DOI: 10.1103/PhysRevD.79.023522 PACS numbers: 98.80.Jk, 98.80.Cq

I. INTRODUCTION

The issue of the initial conditions of our present Universe is connected to the problem of the initial singularity and to the possible solutions adopted to circumvent this problem, which lie in the realm of a quantum theory of gravitation. In fact we may consider that the initial conditions of our present expanding Universe were fixed when the early Universe emerged from a Planckian regime and started its classical evolution. However, by evolving back the initial conditions using Einstein classical equations the Universe is driven toward a singular point where the classical regime is no longer valid. This is an indication that classical general relativity is not a complete theory and in this domain quantum processes must be taken into account. Therefore, initial conditions from which our classical Universe evolved should crucially depend on the version of quantum gravity theory adopted to describe the dynamics in the neighborhood of the classical singularity. This implies that recent observational results in cosmology could in principle guide us in narrowing the possibilities of choices. Inflationary cosmology, for instance, although a highly appealing theoretical paradigm, relies on assumptions about how the Universe emerged from the cosmic singularity. In this vein, models for a preinflationary phase, including quantum corrections and consistent with the inflationary paradigm, are important to be examined.

Among several propositions to describe the dynamics in this preinflationary semiclassical domain are, for instance, quantum loop cosmology [1] and the string based formalism of *D* branes [2], both of them leading to corrections in Einstein's equations and encompassing general relativity as a classical (low energy) limit. In the case of spatially homogeneous and isotropic cosmologies, the basic resulting distinction between the two approaches lies in the corrections introduced in Friedmann's Hamiltonian constraint: quantum loop cosmology leads to corrections in the kinetic energy term of matter fields while bulk-brane corrections lead to extra potential energy terms. In both cases we may have bounces in the scale factor corresponding to the avoidance of a singularity in the models.

In the present paper we adhere to the string based formalism of *D* branes. In this scenario extra dimensions are introduced, the bulk space, and all the matter in the Universe would be trapped on a brane with three spatial dimensions; only gravitons would be allowed to leave the surface and move in the full bulk [3]. At low energies general relativity is recovered but at high energies signifi-

cant changes are introduced in the gravitational dynamics. Our main interest here is connected to the high-energy/quantum corrections that are dominant in the neighborhood of the singularity, resulting in a repulsive force that avoids the singularity and leads the Universe to undergo nonsingular bounces. An elegant geometrical derivation of braneworld dynamics embedded in five-dimensional spacetimes may be found in Refs. [4,5] where both high-energy local corrections as well as nonlocal bulk corrections on a Friedmann-Robertson-Walker (FRW) brane are analyzed. Bouncing braneworld models were constructed by Shtanov and Sahni [6] based upon a Randall-Sundrum type action with one extra timelike dimension.

Here, we examine the full nonlinear dynamics of spatially closed FRW preinflationary braneworld models with a massive scalar field (the inflaton) and several noninteracting perfect fluids. The matter fields evolve on the brane, where high-energy/quantum gravity corrections due to the bulk are included and implement nonsingular bounces. We have previously approached analogous models with a radiation fluid plus a scalar field in the form of small perturbations, where the brane corrections were due to the radiation fluid only or to a phantom-type fluid [7].

With the full nonlinear dynamics new possibilities for cosmological scenarios arise, as nonsingular oscillatory bouncing cosmologies sourced with a pure scalar field, or with a scalar field plus several perfect fluid components that allow to model the effect of dark matter together with barionic matter in the gravitational dynamics. Such nonsingular oscillatory solutions have the theoretical advantage of avoiding the problem of initial conditions at past infinity occurring with one-single bounce solutions and, further, are favored by entropy considerations. We make a detailed examination of nonlinear parametric resonance mechanisms that are present in the full dynamics and turn these bounded oscillatory solutions metastable allowing the model to emerge naturally into an inflationary phase. We consider the restriction such mechanisms impose on the initial configurations so that the models may realize inflation.

We organize the paper as follows. In Sec. II, we give a brief introduction to the framework of the braneworld formulation, making explicit the assumptions used in obtaining the dynamics, and derive the full dynamical equations of the models. In Sec. III, we describe some basic structures (as critical points, invariant planes, and attractors at infinity) that constitute the skeleton of phase space and allow to organize the dynamics in phase space. In Sec. IV, we restrict the matter content of the models to a massive scalar field plus dust and radiation, which constitute a minimal set of ingredients appropriate for a preinflationary model, and analyze the constraints on the parameters of the model so that the dynamics may allow for bounded oscillatory bouncing solutions. In Secs. V and VI we make a semi-analytical approach to nonlinear resonance phenomena in the models that may turn the oscillatory bounded solutions into metastable ones, with an inflationary behavior, and we construct the resonance charts of the dynamics. In Sec. VII, we treat the case of bouncing cosmologies sourced by a pure scalar field. Section VIII is devoted to the exam of the dynamics of initial condition sets connected to a chaotic exit to inflation. Section IX contains the conclusions and final discussions. Throughout the paper we use units such that $\hbar = c = 1$.

II. THE MODEL AND ITS DYNAMICS

Our task here is to derive the full nonlinear dynamical equations of the models, (actually a four-dimensional autonomous dynamical system with one first integral) and to analyze structure of the associated phase space. In the framework of D-brane formalism, we consider a closed FRW metric on the four-dimensional braneworld embedded in a five-dimensional conformally flat bulk. The matter content of the models is constituted of a scalar field ϕ plus several noninteracting perfect fluids, each with equation of state $p_i = \alpha_i \rho_i$. These matter fields are constrained to propagate on the brane only.

We start by giving a brief introduction to braneworld theory, making explicit the specific assumptions used in obtaining the dynamics of the model. We rely on Refs. [5,6], and our notation basically follows [8]. Let us start with a four-dimensional Lorentzian brane Σ with metric g_{ab}, embedded in a five-dimensional conformally flat bulk $\mathcal{M}$ with metric g_{AB}. Capital Latin indices range from 0 to 4, small Latin indices range from 0 to 3. We regard Σ as a common boundary of two pieces $\mathcal{M}_1$ and $\mathcal{M}_2$ of $\mathcal{M}$ and the metric g_{ab} induced on the brane by the metric of the two pieces should coincide although the extrinsic curvatures of σ in $\mathcal{M}_1$ and $\mathcal{M}_2$ are allowed to be different. The action for the theory has the general form

$$S = \frac{1}{2\kappa_5}\Big[\int_{\mathcal{M}_1}({}^{(5)}R - 2\Lambda_5) + 2\epsilon\int_\Sigma K_1 + \int_{\mathcal{M}_2}({}^{(5)}R - 2\Lambda_5) - 2\epsilon\int_\Sigma K_2\Big] + \frac{1}{2}\int_\Sigma\Big(\frac{1}{\kappa_4}{}^{(4)}R - 2\sigma\Big) + \int_\Sigma L_4(g_{ab}, \rho, \phi). \quad (1)$$

In the above ${}^{(5)}R$ is the Ricci scalar of the Lorentzian five-dimensional metric g_{AB} on $\mathcal{M}$, Λ_5 is the five-dimensional cosmological constant, and ${}^{(4)}R$ is the scalar curvature of the induced metric g_{ab} on Σ. The parameter σ is denoted the brane tension, and κ_5 and κ_4 are Einstein constants in five and four dimensions, respectively. The unit vector n^A normal to the boundary Σ has the norm ϵ. If $\epsilon = -1$, the signature of the bulk space is $(-, -, +, +, +)$, so that the extra dimension is timelike. The quantity $K = K_{ab}g^{ab}$ is the trace of the symmetric tensor of extrinsic curvature $K_{ab} = Y_{,a}{}^C Y_{,b}{}^D \nabla_C n_D$, where $Y^A(x^a)$ are the embedding functions of Σ in $\mathcal{M}$ [6]. Also,

$$L_4 = \sqrt{-g}\left[\sum_i \rho_i - \frac{1}{2}(g^{ab}\phi_{,a}\phi_{,b} + m^2\phi^2) - \frac{\xi}{2}{}^{(4)}R\phi^2\right] \tag{2}$$

is the Lagrangean density of the four-dimensional massive inflaton field ϕ plus the perfect fluids (with equation of state $p_i = \alpha_i\rho_i$), whose dynamics is restricted to the brane Σ. They interact only with the induced metric g_{ab}. We further assume that the inflaton field is nonminimally coupled with g_{ab}, with coupling parameter ξ. All integrations over the bulk and the brane are taken with the natural volume elements $\sqrt{-\epsilon^{(5)}g}d^5x$ and $\sqrt{-{}^{(4)}g}d^4x$, respectively.

Variations that leave the induced metric on Σ intact result in the equations

$${}^{(5)}G_{AB} + \Lambda_5 g_{AB} = 0, \tag{3}$$

while considering arbitrary variations of g_{AB} and taking into account (3) we obtain

$${}^{(4)}G_{ab} + \epsilon\frac{\kappa_4}{\kappa_5}(S^{(1)}_{ab} - S^{(2)}_{ab}) = \kappa_4(\tau_{ab} - \sigma g_{ab}), \tag{4}$$

where $S_{ab} \equiv K_{ab} - Kg_{ab}$. τ_{ab} is the energy-momentum tensor of the matter fields on the brane, resulting from (2). In the limit $\kappa_4 \to \infty$ Eq. (4) reduces to the Israel-Darmois junction condition [9]

$$(S^{(1)}_{ab} - S^{(2)}_{ab}) = \epsilon\kappa_5(\tau_{ab} - \sigma g_{ab}). \tag{5}$$

We impose the Z_2 symmetry [5] and use the junction conditions (5) to determine the extrinsic curvature on the brane

$$K_{ab} = -\frac{\epsilon}{2}\kappa_5\left[\left(\tau_{ab} - \frac{1}{3}\tau g_{ab}\right) + \frac{\sigma}{3}g_{ab}\right]. \tag{6}$$

Now, using Gauss equation ${}^{(4)}R_{abcd} = {}^{(5)}R_{MNRS}Y^M_{,a}Y^N_{,b}Y^R_{,c}Y^S_{,d} + \epsilon(K_{ac}K_{bd} - K_{ad}K_{bc})$ together with Eqs. (3) and (6) we arrive at the induced field equations on the brane

$${}^{(4)}G_{ab} = -\left(\frac{\Lambda_5}{2} + \frac{1}{12}\kappa_5^2\epsilon\sigma^2\right)g_{ab} + \frac{\kappa_5^2}{6}\epsilon\sigma\tau_{ab} + \epsilon\kappa_5^2\pi_{ab}. \tag{7}$$

In the above

$$\pi_{ab} = -\tfrac{1}{4}\tau_{ac}\tau^c_b + \tfrac{1}{12}\tau\tau_{ab} + \tfrac{1}{8}g_{ab}\tau_{cd}\tau^{cd} - \tfrac{1}{24}g_{ab}\tau^2. \tag{8}$$

We remark the absence of the conformal tensor projection in Eq. (7) since the four-dimensional brane is embedded in a conformally flat bulk, which is the case of the FRW brane to be considered. Accordingly Codazzi's equations imply that

$$D_a\tau^a_b = 0, \tag{9}$$

where D_a is the covariant derivative with respect to the induced metric g_{ab}. Together with the contracted Bianchi's identities in (7) it results $D_a\pi^a_b = 0$, which corresponds to a sufficient condition for g_{ab} to be embedded in a conformally flat bulk.

Eqs. (7) and (9) are the dynamical equations of the gravitational field on the brane. In Eq. (7) we identify

$$\Lambda_4 = \left(\frac{\Lambda_5}{2} + \frac{1}{12}\kappa_5^2\epsilon\sigma^2\right), \qquad G_N = \frac{\kappa_5^2\sigma\epsilon}{48\pi}, \tag{10}$$

respectively, as the effective cosmological constant, and the effective Newton's gravitational constant in the brane. Both depend basically on the brane tension σ. Equation (7) is similar to Einstein equations in four dimensions, except by the second term in the right-hand side (RHS) that is a correction resulting from the brane-bulk interaction quadratic in the extrinsic curvature, while Eq. (9) is the conservation law for the matter on the brane. We recall that for the evaluation of the extrinsic curvature (6) we use the energy-momentum of the matter fields on the brane. In our model they are described by the Lagrangean density (2).

Let us consider the FRW metric on the brane given by the line element

$$ds^2 = -dt^2 + a(t)^2\left[\frac{dr^2}{1 - kr^2} + r^2(d\theta^2 + \sin^2\theta d\phi^2)\right], \tag{11}$$

where $a(t)$ is the scale factor. For the noninteracting perfect fluids considered in (2), each with equation of state $p_i = \alpha_i\rho_i$, we have then

$$\rho_i = \frac{E_i}{a^{3(1+\alpha_i)}}, \tag{12}$$

where E_i is a constant of motion. The components of the tensor π_{ab} [cf. (8)] are now expressed as

$$\pi_{00} = \frac{1}{12}\left\{\sum_i \rho_i + \rho_\phi + \Delta\right\}^2, \tag{13}$$

$$\pi_{ij} = \frac{1}{12}\left\{\sum_i \rho_i + \rho_\phi + \Delta\right\}^2 g_{ij} + \frac{1}{6}\left\{\sum_i \rho_i + \rho_\phi + \Delta\right\} \times \left\{\sum_i p_i + p_\phi + 2\xi\left[(m^2 + \xi R)\phi^2 - \dot\phi^2 + \frac{\dot a}{a}\phi\dot\phi\right] - \xi\phi^2\left(2\frac{\ddot a}{a} + \frac{\dot a^2}{a^2} + \frac{k}{a^2}\right)\right\}g_{ij}, \tag{14}$$

where

$$\rho_\phi = \tfrac{1}{2}(\dot\phi^2 + m^2\phi^2),\ p_\phi = \tfrac{1}{2}(\dot\phi^2 - m^2\phi^2), \tag{15}$$

$$\Delta = 3\xi\left[\left(\frac{\dot a^2}{a^2} + \frac{k}{a^2}\right)\phi^2 + 2\frac{\dot a}{a}\phi\dot\phi\right], \tag{16}$$

and the curvature scalar $R = 6[\ddot a/a + (\dot a/a)^2 + k/a^2]$. The equations of motion (7) and (9) reduce then to

$$\left(\frac{\dot{a}}{a}\right)^2+\frac{k}{a^2}-\frac{\Lambda_4}{3}=\frac{8\pi G_N}{3}\Big[\sum_i\rho_i+\frac{1}{2}\dot{\phi}^2+\frac{1}{2}m^2\phi^2+3\xi\left(\left(\frac{\dot{a}}{a}\right)^2+\frac{k}{a^2}\right)\phi^2+6\xi\frac{\dot{a}}{a}\phi\dot{\phi}\Big]+\frac{\epsilon\kappa_5^2}{36}\Big[\sum_i\rho_i+\frac{1}{2}\dot{\phi}^2+\frac{1}{2}m^2\phi^2+3\xi\left(\left(\frac{\dot{a}}{a}\right)^2+\frac{k}{a^2}\right)\phi^2+6\xi\frac{\dot{a}}{a}\phi\dot{\phi}\Big]^2, \tag{17}$$

$$\ddot{\phi}+3\frac{\dot{a}}{a}\dot{\phi}+m^2\phi+6\xi\left[\frac{\ddot{a}}{a}+\left(\frac{\dot{a}}{a}\right)^2+\frac{k}{a^2}\right]=0, \tag{18}$$

respectively. Equation (18) is the Klein-Gordon (KG) equation for the inflaton field ϕ while Eq. (17) is the (0,0) equation in (7). Equation (17) is in fact a first integral of the (i, j) equations provided the KG equation holds.

The nonminimal coupling of the inflaton with gravitation considered here is partly motivated by quantum calculations in curved spacetimes (taking into account quantum backreaction, renormalization, etc.) and partly by enlarging the possibilities of constructing successful inflationary and preinflationary scenarios (cf. for instance [10]). The case $\xi=0$ is the usual minimal coupling of the scalar field with gravitation, and $\xi=1/6$ is the so-called conformal coupling [11].

It is not difficult to see from Eq. (17) that the choice $\epsilon=-1$ (corresponding to the extra dimension with timelike character) will implement nonsingular bounces in the dynamics of the scale factor a, implying that the models are nonsingular. In this case, the brane tension σ is required to be negative in order that the subsequent evolution of the Universe be compatible with observations [cf. Equation (10)].

In the remaining of the paper we will restrict ourselves to the case $\epsilon=-1$ and positively curved FRW universes ($k>0$), as we are interested in preinflationary nonsigular dynamics with metastable oscillatory behavior. Partly for analytical and numerical simplicity we will also restrict our analysis to the case of conformal coupling $\xi=1/6$. The basic features of this case encompass that of the minimal coupling case $\xi=0$. Arbitrary ξ's correspond to a higher dimensional parameter space, the scope of which is beyond the purpose of the present paper. The case of pure scalar field bouncing cosmologies will demand a separate treatment, and will be dealt with in Sec. VII. Finally, for numerical computation purposes we fix $\kappa_5^2=6$ and $k=1$.

Within the above restrictions, using the conformal time variable τ (defined by $d\tau=dt/a$) and the rescaled scalar field $\varphi=a\phi$, Eqs. (17) and (18) simplify to

$$a'^2+a^2-\frac{\Lambda_4}{3}a^4=\frac{|\sigma|}{3}\Gamma(\rho_i,\varphi)-\frac{1}{6a^4}[\Gamma(\rho_i,\varphi)]^2, \tag{19}$$

where

$$\Gamma(\rho_i,\varphi)\equiv\left[a^4\sum_i\rho_i+\frac{1}{2}(\varphi'^2+(1+m^2a^2)\varphi^2)\right], \tag{20}$$

and

$$\varphi''+(1+m^2a^2)\varphi=0, \tag{21}$$

where a prime denotes a derivative with respect to the conformal time τ. Equations (19) and (21) constitute the basic dynamical equations to be dealt with in this paper, defined in the phase space $(a, \varphi, a', \varphi')$.

We note that for $m=0$ the dynamics is separable and, as a consequence, integrable. The Klein-Gordon Eq. (21) has the first integral $\mathcal{E}_\varphi^0=(\varphi'^2+\varphi^2)/2$ in this case.

III. THE SKELETON OF PHASE SPACE

From the above Eqs. (19) and (21) we derive the dynamical system

$$\varphi'=p_\varphi,\qquad p_\varphi'=-(1+m^2a^2)\varphi,\qquad a'=p_a/6,$$

$$p_a'=-6a+4\Lambda_4a^3-|\sigma|\Big[\sum_i(3\alpha_i-1)\frac{E_i}{a^{3\alpha_i}}-m^2a\varphi^2\Big]+\Big[\sum_i\frac{E_i}{a^{3\alpha_i+1}}+\frac{1}{2a^2}(\varphi'^2+(1+m^2a^2)\varphi^2)\Big]\times\Big[\sum_j(3\alpha_j+1)\frac{E_j}{a^{3\alpha_j+2}}+\frac{1}{a^3}(\varphi'^2+\varphi^2)\Big]. \tag{22}$$

The first and third Eqs. (22) are mere redefinitions. (p_a, a) can be shown to be canonically conjugated (cf. description of the invariant plane dynamics, for instance). This is not the case of (p_φ, φ), since the first integral (19) is not a Hamiltonian constraint in these variables due the presence of fourth-order powers in φ'.

Three basic structures organize the dynamics in the phase space of the above dynamical system, namely, (i) an invariant plane, (ii) critical points, and (iii) separatrices, allowing us to give a global description of the motion of the models.

The invariant plane is defined by

$$\varphi=0,\qquad p_\varphi\equiv\varphi'=0, \tag{23}$$

where the dynamics is integrable; orbits with initial conditions in this plane are totally contained in it, actually being similar to the dynamics in the sector (a, p_a) of the separable case. A first integral of motion is given by the Hamiltonian constraint

$$\frac{p_a^2}{12}+V(a)-|\sigma|E_{\rm rad}=0, \tag{24}$$

where the potential $V(a)$ is defined as

$$V(a)=3a^2-\Lambda_4a^4-|\sigma|\sum_{i\neq\rm rad}\frac{E_i}{a^{3\alpha_i-1}}+\frac{1}{2}\left(\sum_i\frac{E_i}{a^{3\alpha_i+1}}\right)^2. \tag{25}$$

The equations of motion are equivalent to Hamilton's equations generated from (24), corresponding to the third and fourth Eqs. (22) restricted to the invariant plane (23).

A careful examination shows that for perfect fluids with $-1/3 < \alpha_i \leq 1$ the last term in the potential (25) acts as an infinite potential barrier and is responsible for the avoidance of the singularity $a = 0$. These potential corrections are equivalent to fluids with negative energy densities. This is in accordance with the fact that indeed quantum effects can violate the classical energy conditions, and may avoid curvature singularities where classical general relativity breaks down [12]. Such quantum violations tend to occur on short scales and/or at high curvatures, which is the case in our present models.

Critical points in the finite region of phase space are stationary solutions of Eqs. (22), namely, the points ($p_\varphi = 0, \varphi = 0, p_a = 0, a = a_{\rm crit}$), at which the RHS of Eqs. (22) vanish. Obviously the critical points are contained in the invariant plane, with $a = a_{\rm crit}$ being the real positive roots of $V'(a) = 0$, where a prime here denotes derivative with respect to a. Depending on the values of the parameters ($\Lambda_4, \sigma, E_i, \alpha_i$) we may have from one to several real positive $a_{\rm crit}$. However, it is not difficult to verify that not all of them satisfy the constraint Eq. (19) and that at most two critical points are present, associated with one minimum and one maximum of $V(a)$. As a matter of fact, this is the case for a fixed Λ_4 and sufficiently bounded values of E_i. These limiting conditions on the E_i have not in general a closed analytical form except for the cases of dust or radiation, and will be dealt with in next section. For $\Lambda_4 = 0$, the dynamical system has one critical point only, corresponding to a minimum of the potential $V(a)$; such configurations are not of interest for us since they corresponding to perpetually nonsingular oscillating universes, a scenario where inflation cannot be realized.

To examine the nature of the critical points, and consequently the nature of the motion in their neighborhood, we linearize the dynamical system (22) about each $a_{\rm crit}$. The resulting 4×4 constant matrix of the linearization has the four eigenvalues

$$\lambda_{1,2} = \pm i\sqrt{1 + m^2 a_{\rm crit}^2}, \qquad \lambda_{3,4} = \pm\sqrt{-V''(a_{\rm crit})/6}. \tag{26}$$

related to the linearized motion about $a_{\rm crit}$ in the sector (φ, p_φ) and in the sector (a, p_a), respectively. This characterizes the minimum of $V(a)$ as a center P_0, with two pairs of complex conjugated imaginary eigenvalues ($V''(a_{\rm crit}) > 0$), and the maximum P_1 as a saddle-center [13] with one pair of real eigenvalues with opposite signs ($V''(a_{\rm crit}) < 0$) and one pair of imaginary eigenvalues. These results can be easily interpreted if we expand the integral of motion (19) about the critical points as

$$\begin{aligned}\mathcal{H} \equiv{}& \frac{1}{12}p_a^2 + \frac{1}{2}V''(a_{\rm crit})(a - a_{\rm crit})^2 \\ &- \frac{|\sigma|}{2}(p_\varphi^2 + (1 + m^2 a_{\rm crit}^2)\varphi^2) \\ &+ E_{\rm crit} - |\sigma|E_{rad} + \mathcal{O}(3) = 0,\end{aligned} \tag{27}$$

where $\mathcal{O}(3)$ denotes higher-order terms in the expansion and $E_{\rm crit} \equiv V(a_{\rm crit})$ is the energy of the respective critical point. In a small neighborhood of the critical point these higher-order terms can be neglected and the motion is separable into the two sectors with approximate constant of motions

$$\begin{aligned}E_{(a)} &= \tfrac{1}{12}p_a^2 + \tfrac{1}{2}V''(a_{\rm crit})(a - a_{\rm crit})^2, \\ E_{(\varphi)} &= \tfrac{1}{2}(p_\varphi^2 + (1 + m^2 a_{\rm crit}^2)\varphi^2),\end{aligned} \tag{28}$$

with $E_{(a)} - |\sigma|E_{(\varphi)} + E_{\rm crit} - |\sigma|E_{rad} \sim 0$ and $|E_{\rm crit} - |\sigma|E_{rad}|$ small. It is immediate to see that the sector associated with $E_{(\varphi)}$ always correspond to rotational motion in the variables (φ, p_φ) about the critical points, while the sector associated with $E_{(a)}$ corresponds to either (i) rotational motion or (ii) hyperbolic motion in the variables (a, p_a) about the respective critical point; namely, the minimum of the potential P_0 corresponds to a center and the maximum P_1 corresponds to a saddle-center, as mentioned before. P_0 and P_1 define, respectively, a stable and an unstable static Einstein universe. The stable Einstein universe configuration has no classical analogue, arising from the dynamical balance between the perfect fluid energy content and the negative energy density connected to the high-energy/quantum corrections in the potential. We are now ready to describe the topology of the motion about the critical points and its extension to a nonlinear neighborhood of these points. This will be done in next section for the case of a preinflationary model containing cold dark matter (dust), dark energy (a positive cosmological constant), and radiation.

Finally, from the saddle-center critical point (when present) there emerges a structure of separatrices $\mathcal{S}$ contained in the invariant plane. One of them tends to a de Sitter attractor at infinity, defining a escape of orbits to the inflationary regime. In fact, a straightforward analysis of the infinity of the phase space shows the presence of a pair of critical points in this region, one acting as an attractor (stable de Sitter configuration) and the other as a repeller (unstable de Sitter configuration). The scale factor approaches the de Sitter attractor as $a(\tau) \sim (C_0 - \tau)^{-1}$ for $\tau \to C_0$, where τ is the conformal time, or as $a(t) \sim \exp(t\sqrt{\Lambda_4/3})$ for $t \to \infty$, where t is the cosmic time.

IV. PRE-INFLATIONARY MODEL WITH DARK MATTER, DARK ENERGY, AND RADIATION

To proceed with our analysis further we will consider braneworld models whose matter content is restricted to a

dark matter component (dust) and radiation, together a massive scalar field (the inflaton) and a dark energy component described by the effective cosmological constant in the brane [cf. Equation (10)]. The reasons for these restrictions are twofold. First the model contains a minimal set of ingredients that is appropriate for a preinflationary model. The second is more technical and has to do with the number of independent perfect fluid components. A large number of fluid components results in a higher dimensional parameter space, what turns the numerical/analytical analysis of parametric resonance quite involved. Furthermore, the resonance patterns that are important for the physics of inflation in this model are typical for the dynamics of the general model as we will discuss later. In this instance Eqs. (19)–(21) reduce then to

$$\frac{p_a^2}{12} + V(a) - |\sigma|E_{\rm rad} - \frac{|\sigma|}{2}(\varphi'^2 + (1+m^2a^2)\varphi^2) + \frac{1}{2a^2}\left(\frac{E_{\rm rad}}{a^2} + \frac{E_{\rm dust}}{a}\right)(\varphi'^2 + (1+m^2a^2)\varphi^2) + \frac{1}{8a^4}(\varphi'^2 + (1+m^2a^2)\varphi^2)^2 = 0, \tag{29}$$

and

$$\varphi'' + (1+m^2a^2)\varphi = 0, \tag{30}$$

where

$$V(a) = 3a^2 - \Lambda_4 a^4 - |\sigma|E_{\rm dust}a + \frac{1}{2}\left(\frac{E_{\rm rad}}{a^2} + \frac{E_{\rm dust}}{a}\right)^2. \tag{31}$$

We remark that for the integrable case $m = 0$, Eq. (29) simplifies to

$$\frac{p_a^2}{12} + \tilde{V}(a) - |\sigma|(E_{\rm rad} + \mathcal{E}_\varphi^0) = 0, \tag{32}$$

where

$$\tilde{V}(a) = 3a^2 - \Lambda_4 a^4 - |\sigma|E_{\rm dust}a + \frac{1}{2}\left(\frac{E_{\rm rad} + \mathcal{E}_\varphi^0}{a^2} + \frac{E_{\rm dust}}{a}\right)^2, \tag{33}$$

with $\mathcal{E}_\varphi^0 \equiv (\varphi'^2 + \varphi^2)/2$ a constant of motion. If we compare Eq. (32) with Eq. (24) for the invariant plane, and Eq. (33) with Eq. (31) we may see that the integrable dynamics ($m = 0$) is analogous to the integrable dynamics in the invariant plane up to the substitution $E_{\rm rad} \to E_{\rm rad} + \mathcal{E}_\varphi^0$. In other words, the integrable scalar field behaves as a radiation fluid in respect to the dynamics of the scale factor, a fact that will be used in Sec. VII, for the case of pure scalar field cosmology. We should remark that in the low energy limit the cosmological constant on the brane Λ_4 may be interpreted as the effective vacuum energy of the inflaton field and φ are the spatially homogeneous expectation values of the inflaton fluctuations about its vacuum state. When these fluctuations are considered small or initially small, namely, taken near the invariant plane, we may neglect $\mathcal{E}_\varphi^0$ and the integrable dynamics $m = 0$ is approximately that of the invariant plane. The scalar field fluctuations will then actually have the role of just triggering the resonances in the perfect fluid cosmologies.

In Fig. 1 we depict the phase space portrait of the integrable dynamics in the invariant plane ($\varphi = 0 = p_\varphi$) for the case of dust and radiation, with $|\sigma|E_{\rm dust}$ sufficiently bounded so that $V(a)$ has a well (we adopted $|\sigma| = 500$ and $E_{\rm rad} = E_{\rm dust} = 10^{-3}$). The critical points P_0 (center) and P_1 (saddle-center) correspond to stable and unstable Einstein universes. Typically the model allows for the presence of perpetually bouncing universes (periodic orbits) in Region I of Fig. 1, associated with motion in the potential well $V(a)$ about the stable Einstein universe configuration P_0. These configurations are basically the ones for which $|\sigma|E_{\rm rad} < V(a_{\rm max})$. Region I, understood as a nonlinear neighborhood of P_0, is bounded by the homoclinic separatrix $\mathcal{S}$ emerging from the saddle-center P_1 [14]. Orbits in Region II are correspond to one-bounce universes. A separatrix emerges from P_1 toward the de Sitter attractor at infinity, defining a escape to inflation.

Finally, it is worth mentioning here some basic structural differences between the integrable dynamics in the invariant plane and that of the integrable case (Eq. (32) and Eq. (30) for $m = 0$) whenever $\varphi(0)$ and/or $p_\varphi(0)$ are not zero. The phase space portrait in the plane (a, p_a) is similar to that of the invariant plane shown in Fig. 1, however, P_1 and P_0 are no longer critical points but periodic orbits. The

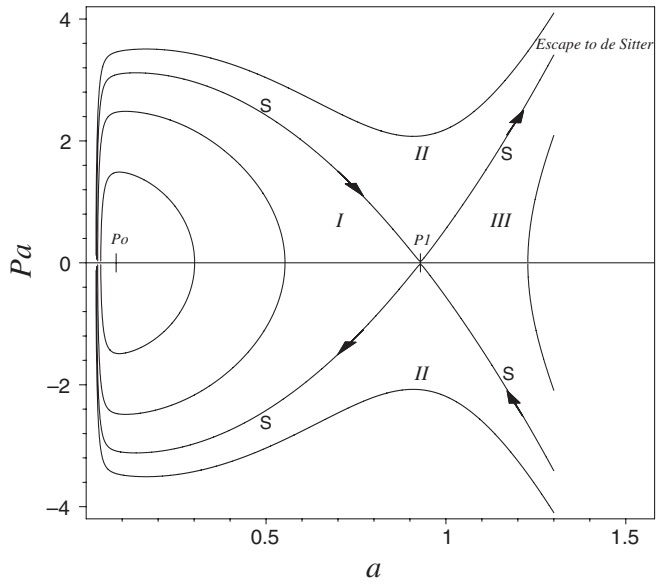

FIG. 1. The phase portrait of invariant plane dynamics with the critical points P_0 (center) and P_1 (saddle-center) corresponding to stable and unstable Einstein universes. The periodic orbits of Region I describe perpetually bouncing universes. Orbits in Region II are solutions of one-bounce universes. A separatrix $\mathcal{S}$ emerges from P_1 toward the de Sitter attractor defining a escape to inflation.

integrable dynamics is not restricted to this plane but, in the case of Region I, evolve on tori that are the direct product of the closed curves in Region I to periodic orbits in the sector (φ, p_φ). In particular, the product of the separatrix $\mathcal{S}$ that bounds the Region I times a periodic orbit with initial conditions fixed by the constant $\mathcal{E}_\varphi^0$ is a cylinder. The orbits on this cylinder coalesce (for times $\tau \to \pm\infty$) to the periodic orbit at P_1 with the same constant of motion. This cylinder is said to be homoclinic to the periodic orbit at P_1.

As we mentioned already, for a fixed value of Λ_4 the potential $V(a)$ has two extrema (one minimum and one maximum) for suitably bounded values of $(|\sigma|, E_{\rm rad}, E_{\rm dust})$, corresponding to a well in the potential. For the case of pure radiation we can show that $V(a)$ will have this well provided that

$$E_{\rm rad}^2 < \frac{2187}{2048}\frac{1}{\Lambda_4^3}. \tag{34}$$

The two extrema of $V(a)$ for this case are critical points of the dynamics since $V(a) > 0$ for all $a > 0$ implying that even the minimum of the potential belongs to the physical phase space domain. For $E_{\rm rad}$ violating the above restriction no extrema are present, and the system has no critical point in the finite region of phase space. For the case of pure dust $V(a)$ has no extrema if

$$|\sigma|E_{\rm dust} > \frac{16\sqrt{3}}{9}\frac{1}{\sqrt{\Lambda_4}}.$$

For radiation plus dust we do not have a closed form for the constraint conditions on the parameters. However, it is not difficult to check that, in general, the increase of $|\sigma|E_{\rm dust}$, namely, the increase of the gravitational interaction strength of the dust component, has the effect of taking the minimum of $V(a)$ out of the physical space leading eventually to a destruction of the well. In other words, the increase of $|\sigma|E_{\rm dust}$ has the effect of reducing the phase space volume available for bounded and/or initially bounded (metastable) configurations. This is illustrated in Fig. 2 where we plot the potential $V(a)$ for several increasing values of $|\sigma|E_{\rm dust}$ with fixed Λ_4 and $E_{\rm rad}$ (as a matter of fact we fixed $\Lambda_4 = 1.5$, $E_{\rm dust} = 0.001$, $E_{\rm rad} = 0.01$ and varied $|\sigma|$). We see that for $|\sigma|E_{\rm dust} \gtrsim 2.3$ the well in the potential is no longer present.

The structure of motion about P_0 will be the main object of our interest in the following. This region is physically more relevant than that of one-bounce models since it avoids the theoretical problems of posing initial conditions at past infinity, this issue being possibly brought to the realm of a semiclassical quantization of the dynamics in the Region I. Furthermore, maximum entropy considerations [15] favor the stable Einstein universe as a suitable past configuration about which initial states of the preinflationary universe oscillate. However, we must provide a mechanism for such bounded and perpetually bouncing universe configurations to become metastable so that they may realize inflation and escape to the de Sitter attractor at infinity. Such a mechanism will be the nonlinear resonance provided by the interaction with the scalar field sector (φ, p_φ) in the nonintegrable case, as we proceed to discuss.

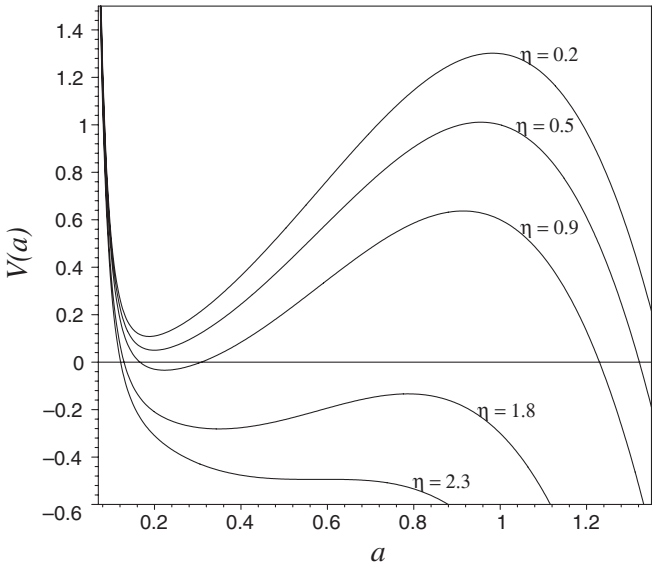

FIG. 2. Plots of the potential $V(a)$ for increasing values of $\eta \equiv |\sigma|E_{\rm dust}$. For higher values of $|\sigma|E_{\rm dust}$ the minimum is out of the physical phase space and eventually disappears (for $|\sigma|E_{\rm dust} \gtrsim 2.3$) together with the potential well.

We should finally remark that the increase of $|\sigma|E_{\rm dust}$, namely, the increase of Newton's constant on the brane and/or the increase of the dust content of the model, have the effect of taking the stable Einstein universe configuration out of the physical phase space (cf. Figure 2); in the latter situation the physical phase space is not simply connected presenting a void with the structure of a solid torus.

V. NONLINEAR RESONANCE OF KAM TORI

We start by discussing the topology of motion about the stable Einstein universe P_0 that includes (i) the structure of KAM tori that are present in the neighborhood of P_0 and arise from the tori of the integrable case $m = 0$; (ii) nonlinear resonance mechanisms inducing that either KAM tori are destroyed by the resonance allowing the orbit escape to the de Sitter attractor or the motion is chaotic (confined between two KAM tori) but otherwise stable.

Let us consider the energy surfaces $|\sigma|(E_{\rm rad} + \mathcal{E}_\varphi^0) < E_{\rm crit}(P_1) \equiv V(P_1)$ corresponding to bounded motion in the integrable case $m = 0$, or to initially bounded motion in the nonintegrable cases. This phase space region can indeed be characterized as a nonlinear neighborhood of the center P_0, and is foliated by the two-tori $\mathcal{S}^1 \times \mathcal{S}^1$ that are the topological product of periodic orbits of the separable sectors (φ, p_φ) and (a, p_a), with the two associated sepa-

rately conserved quantities $\mathcal{E}^0_\varphi$ and $\mathcal{E}^0_a = (p_a^2/12 + \tilde{V}(a))$ satisfying $\mathcal{E}^0_a - |\sigma|(E_{\rm rad} + \mathcal{E}^0_\varphi) = 0$. The frequency ν_a of the periodic orbit in the sector (a, p_a) is given by the third-kind elliptic integral [16]

$$\frac{1}{\nu_a} = \sqrt{\frac{12}{\Lambda_4}} \int_{\beta_3}^{\beta_2} \frac{x^2 dx}{\sqrt{(x^2 - 2\alpha_1 x + (\alpha_1^2 + \alpha_2^2)) \prod_{i=1}^{6} (x - \beta_i)}}, \tag{35}$$

where $(\beta_i, i = 1 \ldots 6)$ and $(\alpha_1 \pm i\alpha_2)$ are, respectively, the real and imaginary roots of $\tilde{V}(a) - |\sigma|(E_{\rm rad} + \mathcal{E}^0_\varphi) = 0$ ($\beta_3 < \beta_2 < \beta_1$ are the positive real roots). The two tori of the integrable case are the topological product of the above class of periodic orbits parametrized by $\mathcal{E}^0_a$ with the periodic orbits of the harmonic oscillator parametrized by $\mathcal{E}^0_\varphi$ (with frequency $\nu_\varphi = 1/2\pi$).

For future reference we note that the periodic orbits of the sector (a, p_a) in the integrable case will be represented by the elliptic fixed point ($\varphi = 0$, $p_\varphi = 0$), namely, the origin of the Poincaré map with surface of section $p_a = 0$, in case $\mathcal{E}^0_\varphi = 0$. For $\mathcal{E}^0_\varphi \neq 0$ the corresponding integrable tori are represented by closed invariant curves about the origin of the map. For a small nonintegrable parameter m this picture is maintained with ($\varphi = 0$, $p_\varphi = 0$) as a center of a primary island of KAM tori; in fact, the KAM theorem [17] establishes the stability of tori with a sufficiently incomensurate frequency ratio, which in the present case means ν_a is sufficiently irrational. Other integrable tori are destroyed by the nonintegrable perturbation, and the region between two remaining invariant tori presents an intricate dynamics (unstable periodic orbits, stable periodic orbits surrounded by islands, broken separatrices, and stochastic layers, this structure repeating down to smaller scales [14]). The importance of KAM tori for Hamiltonian systems with two degrees of freedom comes from the fact that they prevent the diffusion of trajectories in the whole phase space, and thus preventing in our model the entrance to inflation. As m increases numerical experiments show that invariant KAM tori may be destroyed, with a consequent loss of stability of the system. This is the case of interest to us as orbits initially trapped about the center ($\varphi = 0$, $p_\varphi = 0$) can escape into the inflationary phase. An important mechanism for this breakup of invariant tori is nonlinear resonance that occurs in a restricted domain of parameters of the system as we proceed to examine using a semi-analytical approach.

If m is small and/or we start from an initial condition $(\varphi_0, p_{\varphi 0})$ small (namely, near the invariant plane) we may approximate Eq. (30) as

$$\varphi'' + (1 + m^2 a_0^2(\tau))\varphi = 0, \tag{36}$$

where $a_0(\tau)$ is a solution of $a'' + dV(a)/da \approx 0$ [cf. Equation (22)]. Equation (36) has the form of a Lamé-type equation, and therefore parametric resonance occurs when the ratio

$$R = \frac{\nu_a}{\tilde{\nu}_\varphi} \tag{37}$$

is a rational number, where [18]

$$\tilde{\nu}_\varphi = \frac{1}{2\pi}\sqrt{1 + \frac{(0.9m)^2}{2}(\beta_3^2 + \beta_2^2)}. \tag{38}$$

Under this condition φ begins to grow exponentially in time and to act on the dynamics of the scale factor a, which in turn will modify (36). This feedback will restructure the resonance, either (i) by leading the dynamics into a more unstable behavior, with amplification of the resonance mechanism and consequent breaking of the KAM tori and escaping of the orbits; or (ii) by leading the orbits to a general chaotic motion in a bounded region of phase space. This general nonlinear resonance mechanism can be given an approximate analytical treatment, through which we can fix the dominant resonances, namely, the rational numbers R corresponding to the dominant resonances. In this approximation, where higher-order terms in (φ, p_φ) are neglected, the first integral (29) is approximated by

$$\mathcal{H} \equiv \mathcal{E}^0_a - |\sigma|\mathcal{E}^0_\varphi - \frac{|\sigma|}{2} m^2 a^2 \varphi^2 \simeq |\sigma| E_{\rm rad}. \tag{39}$$

Further, in the remaining nonintegrable term the variable a and φ are substituted by the integrable solutions $a_0(\tau)$ and $\varphi_0(\tau)$. Since the Hamiltonian character of the first integral is recovered in the approximation, we are led to introduce action-angle variables $(\mathcal{J}_a, \Theta_a, \mathcal{J}_\varphi, \Theta_\varphi)$, the angle variables being defined as $(\Theta_a = \nu_a \tau$, $\Theta_\varphi = \tilde{\nu}_\varphi \tau)$ such that both Θ_a and Θ_φ vary in the interval $[0, 1]$ during a complete cycle of the original variables. We remark that in the numerical experiments considered we have $\mathcal{E}^0_a \approx |\sigma| E_{\rm rad}$ in the initial stages of the dynamics. $\mathcal{E}^0_a$ is however not conserved as the dynamics proceeds, the nonintegrable term being responsible for the exchange of energy with the sector (φ, p_φ). Taking into account that the function $a_0(\tau)$ is periodic with period $T_a = \nu_a^{-1}$, the expansion in circular functions of the nonintegrable term of (39) takes the form [16]

$$\mathcal{H}_i = -\frac{|\sigma|}{2} m^2 \mathcal{J}_a^{(0)} \mathcal{J}_\varphi^{(0)} \sum_n (A_n \cos 2n\pi\Theta_a) \cos 4\pi\Theta_\varphi, \tag{40}$$

where A_n are numerical coefficients depending the parameters of the model through the roots of $V(a) - |\sigma| E_{\rm rad} \sim 0$ [cf. Equation (35)], and a zero superscript denotes action variables of the integrable case. Hamilton's equation for $\mathcal{J}_a$ derived from (39) can be integrated for each given term n of the series, yielding to a first approximation

$$\mathcal{J}_a \sim \frac{|\sigma|}{2} m^2 \mathcal{J}_a^{(0)} \mathcal{J}_\varphi^{(0)} \sum_n \frac{A_n}{2\pi n \tilde{\nu}_\varphi} \left[\frac{\cos(2\pi n \Theta_a - 4\pi \Theta_\varphi)}{R - 2/n} + \frac{\cos(2\pi n \Theta_a + 4\pi \Theta_\varphi)}{R + 2/n} \right]. \quad (41)$$

From (41) we have that the dominant terms are the ones for which $R \simeq 2/n$. Therefore, for a fixed $n \geq 2$ the expression

$$R = \frac{\nu_a}{\tilde{\nu}_\varphi} = \frac{2}{n}, \qquad n \geq 2 \quad (42)$$

determines a volume in the parameter space $(|\sigma|, E_{\rm rad}, E_{\rm dust}, m)$ in the neighborhood of which a n-resonance occurs. It represents a further step beyond the analysis of resonances (37) in the linear regime of Lamé-type Eq. (36). The setup of the resonance is signaled by the bifurcation of the periodic orbit at the origin ($\varphi = 0$, $p_\varphi = 0$) into an unstable periodic orbit plus one or two characteristic stable periodic orbits of the resonance (according, respectively, whether n is odd or even), a fact crucial to realize inflation, as we will discuss later.

The resonance chart for the model can now be constructed numerically using the exact dynamics. Expression (42)—where approximations as well as the neglect of nonresonant terms were used—constitutes an accurate guide to localize and label the resonances in the parameter space (obviously for a fixed Λ_4, the values of $|\sigma| E_{\rm dust}$ and E_0 must be compatible with initially bounded motion). However, in the actual chart of resonance constructed numerically using the exact dynamics, these domains will have a spread that is a correction of the approximations due the full dynamics.

The focus on the underlying bulk-brane structure of the gravitational dynamics will lead us to examine initially the plane (σ, m) of the parameter space, while fixing the total mass energy of dust $E_{\rm dust}$ and of radiation $E_{\rm rad}$ in several distinct ratios. For numerical purposes in all numerical experiments we will fix $\Lambda_4 = 1.5$.

Figure 3 displays the resonant chart in the plane (σ, m) of the parameter space for fixed $E_{\rm dust} = E_{\rm rad} = 10^{-3}$. The chart correspond to initial conditions taken near the invariant plane, namely, near the periodic orbit at the origin ($\varphi = 0$, $p_\varphi = 0$), with $p_a = p_\varphi = 0$, $\varphi = 10^{-4}$. The continuous lines are solutions of (42), while the gray regions spreading about the lines are sections of the resonance windows by the planes $E_{\rm dust} = 0.001$, $E_{\rm rad} = 0.001$. The remaining (white) regions are domains of stable motion, with the dynamics bounded by KAM tori. We restricted ourselves up to the resonance $n = 5$ in order to not overcrowd the figure. On driving the system toward a resonance zone (by an appropriate change of m and/or $|\sigma|$) we can turn a stable configuration into a metastable one with consequent escape of the orbits to the de Sitter attractor at infinity in a finite time. In the realm of our pre-inflationary models, stability versus nonlinear resonance instability will be considered connected to initial conditions near the invariant plane

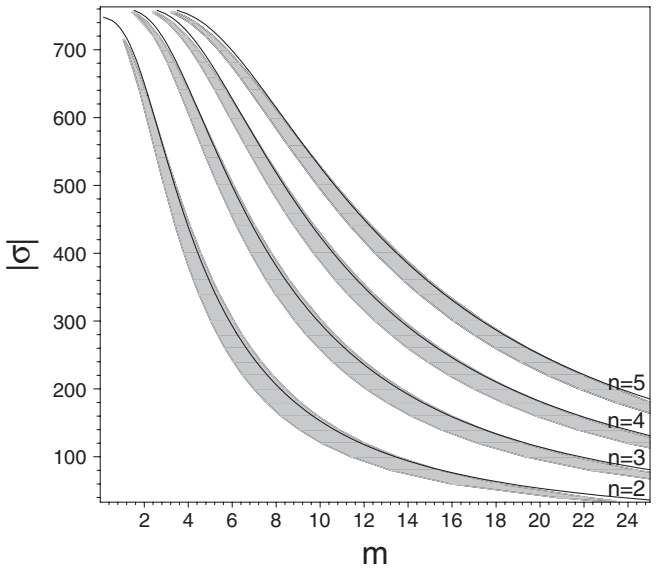

FIG. 3. Resonance chart in the plane (σ, m) for $E_{\rm rad} = E_{\rm dust} = 10^{-3}$ and $\varphi_0 = 10^{-4}$. The continuous lines are solutions of the approximate resonant condition (42), while the gray regions about the lines are the parametric resonance windows for the exact dynamics, corresponding to the bifurcation of the periodic orbit at the origin. The white regions correspond to KAM stable motion.

only, namely, with (φ, p_φ) small, corresponding to spatially homogeneous fluctuations of the inflaton field. Nonlinear resonance will turn orbits generated from these initial conditions from stable to unstable (and *vice versa*) as a consequence of bifurcation of the critical point ($\varphi = 0$, $p_\varphi = 0$), at the origin of the Poincaŕe map with surface of section $p_a = 0$, from a center to a saddle (and *vice versa*), breaking up the KAM tori that trap the orbits about the origin. We recall that the origin of the map is a periodic orbit of period $1/\nu_a$ in the (a, p_a) sector. This is illustrated by the two Poincaré maps of Fig. 4 with surface of section $p_a = 0$, for $E_0 = E_1 = 10^{-3}$ and $|\sigma| = 500$ fixed, and $m = 5.85$ in the domain of parametric resonance $n = 3$ (top map), and $m = 7.1$ in the domain of parametric stability between the resonances $n = 3$ and $n = 4$ (bottom map). The origin in the top map is a saddle, with two associated centers, a consequence of the bifurcation of the periodic orbit at the origin due to the resonance $n = 3$. No KAM tori is present about the origin of the map so that orbits with initial conditions about the origin are not trapped and free to escape for large regions of phase space and eventually reach the de Sitter attractor at infinity, realizing inflation. The parametric domain of resonance thus favor inflation. The origin of the bottom map is a center, enclosed by KAM tori that trap the orbits with initial conditions in this neighborhood, forbidding escape to the de Sitter infinity. Therefore, the region of parametric stability of the system will be unfavorable to the physics of inflation since the orbit (a configuration of the early uni-

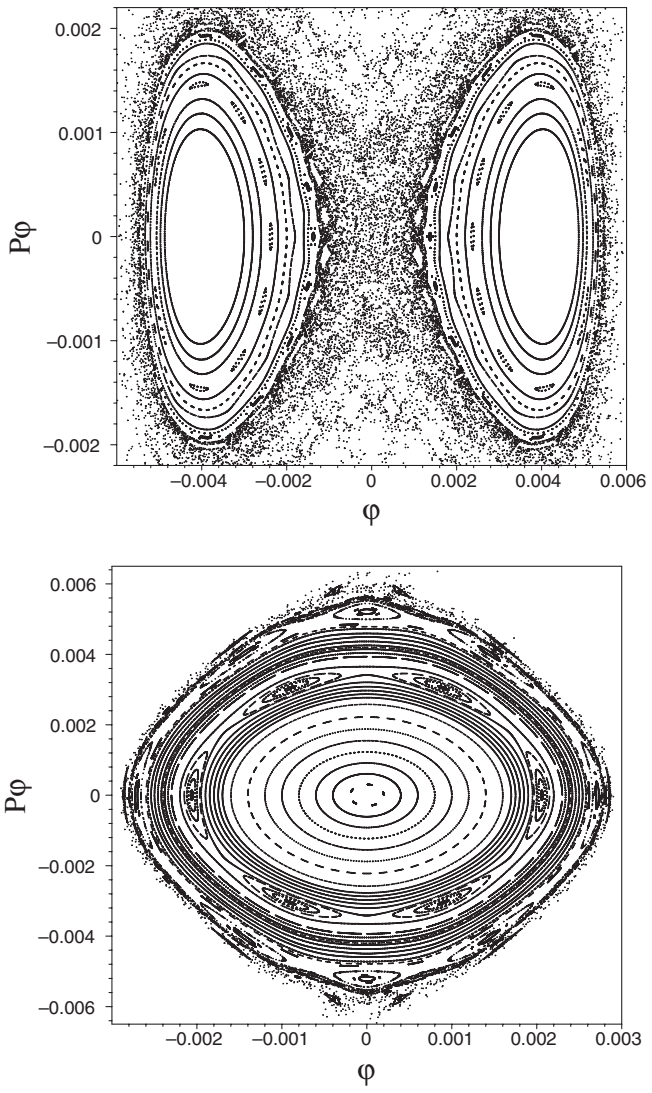

FIG. 4. Poincaré maps with surface of section $p_a = 0$ for ($|\sigma| = 500$, $m = 5.85$) in the domain of parametric resonance $n = 3$ (top), and ($|\sigma| = 500$, $m = 7.1$) in the domain of parametric stability between the resonances $n = 3$ and $n = 4$ (bottom). The origin in the top map is a saddle, connected to the bifurcation of the origin due to the resonance $n = 3$, favoring inflation. The bottom map has a center at the origin, enclosed by KAM tori that trap the inflaton, preventing inflation.

verse) will be trapped in a stable state between two KAM tori about the center at the origin. The structure of the stochastic sea is distinct in each case. If the system is in the region of parametric resonance, initial conditions near the invariant plane may undergo a long-time diffusion through the stochastic sea to large regions of phase space, and finally escape to the de Sitter attractor. On the other hand, when the system is in the region of parametric stability initial conditions for orbits that diffuse are far from the origin, beyond the borders of the main island of the map, and diffusion with escape to de Sitter infinity is extremely rapid.

Numerical experiments with the exact dynamics show that the presence of dust has the effect of squeezing the volume of the resonance windows, being thus less favorable to the occurrence of inflation. In Fig. 5 we show the resonance windows $n = 3$, corresponding to $\varphi_0 = 10^{-4}$, for fluid content with pure dust ($E_{\rm rad} = 0$, $E_{\rm dust} = 0.001$), pure radiation ($E_{\rm rad} = 0.001$, $E_{\rm dust} = 0$), and a mixture of both ($E_{\rm rad} = E_{\rm dust} = 0.001$), the latter already shown in Fig. 3. Their range in the parameter space and relative size are distinct, the available width for a fixed σ being much reduced when dust is present. For reference we give the width Δm of $n = 3$ resonances windows for $|\sigma| = 600$ and $|\sigma| = 400$, and for several distinct matter content:

	$E_{\rm rad} = 10^{-3}$ $E_{\rm dust} = 0$	$E_{\rm rad} = 10^{-3}$ $E_{\rm dust} = 10^{-4}$	$E_{\rm rad} = 10^{-3}$ $E_{\rm dust} = 10^{-3}$	$E_{\rm rad} = 0$ $E_{\rm dust} = 10^{-3}$
Δm ($\|\sigma\| = 600$)	1.1088	1.0446	0.51 665	0.55 880
Δm ($\|\sigma\| = 400$)	1.4418	1.3850	0.9307	1.1305

Hence, if we demand that dark matter is present as a dust fluid in this pre-inflationary phase then its total mass-energy content must not be exceedingly large in comparison with the radiation content in order that inflation be properly realized. In addition, we recall that, as discussed in Sec. IV, the presence of dust has the effect of reducing the available phase space volume for bounded and/or initially bounded (metastable) configurations about the Einstein stable universe, as regulated by $|\sigma| E_{\rm dust}$.

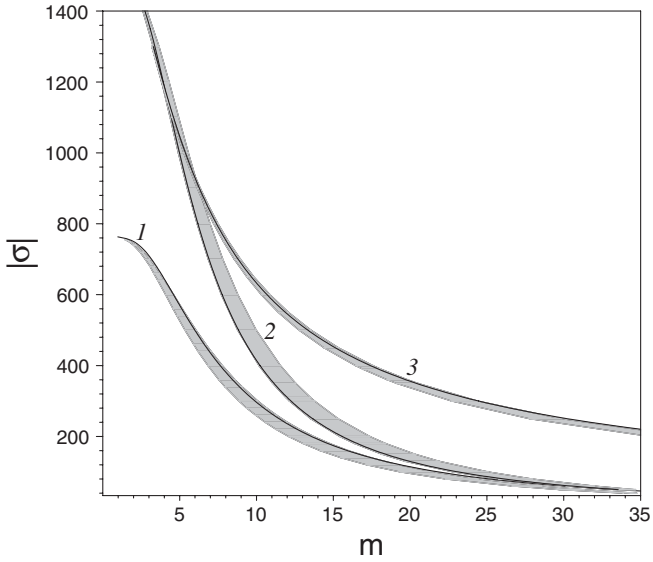

FIG. 5. Resonance windows $n = 3$ for (1) dust plus radiation ($E_{\rm rad} = E_{\rm dust} = 10^{-3}$), (2) pure radiation ($E_{\rm rad} = 10^{-3}$, $E_{\rm dust} = 0$), and (3) pure dust ($E_{\rm rad} = 0$, $E_{\rm dust} = 10^{-3}$). The range and relative size of the windows are distinct, the case of pure dust having a relative smaller volume though a more extended region of parameters. The presence of dust has the effect of squeezing the width of the resonance windows, reducing the domain of favorable configurations to realize inflation as concerning the parametric resonance mechanism.

Summarizing, the instability versus the stability of the origin ($\varphi = 0,\ p_\varphi = 0$) is crucial for the dynamics of inflation, having a bearing on the dynamics of the spatially homogeneous expectation values $\varphi(\tau)$ of the inflaton field related to the escape into inflation. In this instance the initial conditions for φ are assumed to be small, and are to be taken near the invariant plane (23), which corresponds to a neighborhood of the critical point of the map at the origin ($\varphi = 0,\ p_\varphi = 0$). Therefore, the region of parametric stability is unfavorable for producing inflation since the orbit (a configuration of the early Universe) will be trapped in a stable state enclosed by two invariant tori of a main KAM island of the map. On the other hand, on driving the system to a region of parametric resonance, orbits with initial conditions near the invariant plane are turn into metastable configurations that either escape rapidly to de Sitter infinity or undergo a long-time diffusion through stochastic regions of phase space before finally escaping. The resonance windows in the complete parameter space ($\sigma, E_{\rm rad}, E_{\rm dust}, m$) are constituted of n disjoint four-dimensional volumes the sections of which—for instance, with the surfaces $E_{\rm rad} = 10^{-3}$ and $E_{\rm dust} = 10^{-3}$—result in the n gray regions of Fig. 3. The volumes of the windows are small as compared to the whole volume of the parameter space, and only initial configurations inside them may realize inflation. We note that for a fixed m the larger the order n of the resonance the stronger the gravitational interaction in the braneworld universe inflated from initial conditions connected with the resonance considered.

VI. A PARTITION IN THE RESONANCE WINDOWS CODED BY DISRUPTIVE RESONANCES

From the point of view of the dynamics of inflation, the resonance windows present a further structure connected with disruptive resonances and/or long-time diffusion before escape to inflation. In fact, as we proceed to discuss, a considerable domain of the resonance windows—although corresponding to a bifurcation of the stable periodic orbit at the origin—does not lead to escape into inflation and must be properly discarded. To simplify our analysis we restrict ourselves to the resonance window $n = 3$ (cf. Figure 3) at fixed $|\sigma| = 350$. The associated range of m lies in the interval $\Delta m \cong [7.78\,431, 8.84\,341]$. A careful numerical examination shows that in this interval of the resonance zone we observe that three dynamically distinct regions are present: (i) the domain on the left, ranging from the lower limit up to $m \lesssim 8.52$, corresponds to configurations for which the dynamics is highly unstable, the resonances being disruptive with a rapid escape to inflation (up to $\tau \leq 15\,000$). (ii) A threshold region $8.52 < m < 8.56$ that corresponds to configurations of orbits that undergo a long-time diffusion ($15\,000 < \tau < 100\,000$) before escaping to inflation. (iii) The region on the right of the threshold, ranging from $m \gtrsim 8.56$ up to the upper limit of Δm. The motion of orbits connected to this latter parametric region—although corresponding to the case of a bifurcated saddle at the origin—is resonant and chaotic, but otherwise stable. Therefore, Region III should be discarded since cosmological scenarios corresponding to these configurations do not properly realize inflation.

The above dynamically distinct behaviors are illustrated as follows. Figure 6 shows the time signals for $m = 7.99$ taken in the region of disruptive resonance; the escape to inflation occurs at $\tau \simeq 140$ and time signals are used since there is not enough recurrence for constructing a well-defined Poincaré map. Figure 7 displays the Poincaré map with surface of section $p_a = 0$ of a single orbit for $m = 8.555$, corresponding to the threshold Region II, undergoing a long-time diffusion before exit to inflation, at $\tau \simeq 64\,000$. Finally, the time signals shown in Fig. 8 correspond to $m = 8.6$ in Region III near the right border of the resonance window $n = 3$. The motion is resonant and chaotic, but otherwise stable. All Figures were generated with $\varphi' = 0 = p_a$, $\varphi = 10^{-4}$.

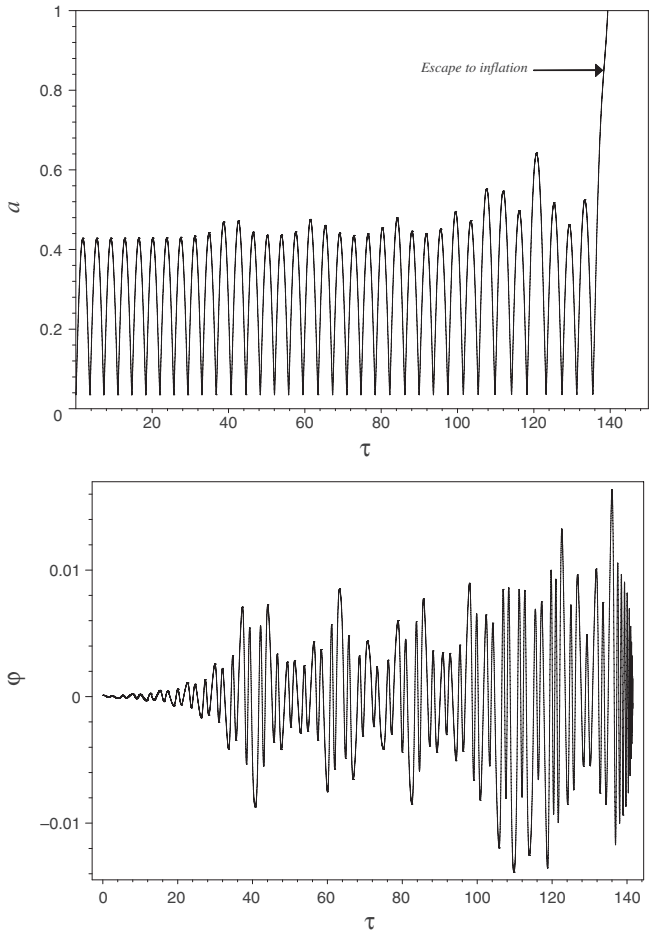

FIG. 6. Time signals for $m = 7.99$ and $|\sigma| = 350$ corresponding to the region of disruptive resonances, near the left border of the $n = 3$ resonance window of Fig. 3.

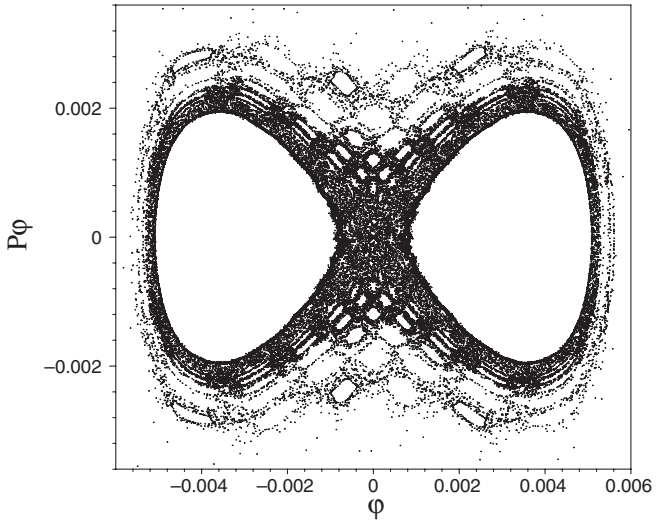

FIG. 7. Poincaré map with surface of section $a' = 0$ of a single orbit, for $m = 8.555$ and $|\sigma| = 350$ in the threshold region of the $n = 3$ resonance window of Fig. 3. The orbit undergoes a long-time diffusion before escape to inflation at $\tau \simeq 64\,000$. The map exhibits the structure of the random motion of the orbit in the stochastic sea about primary and secondary KAM islands of the resonance.

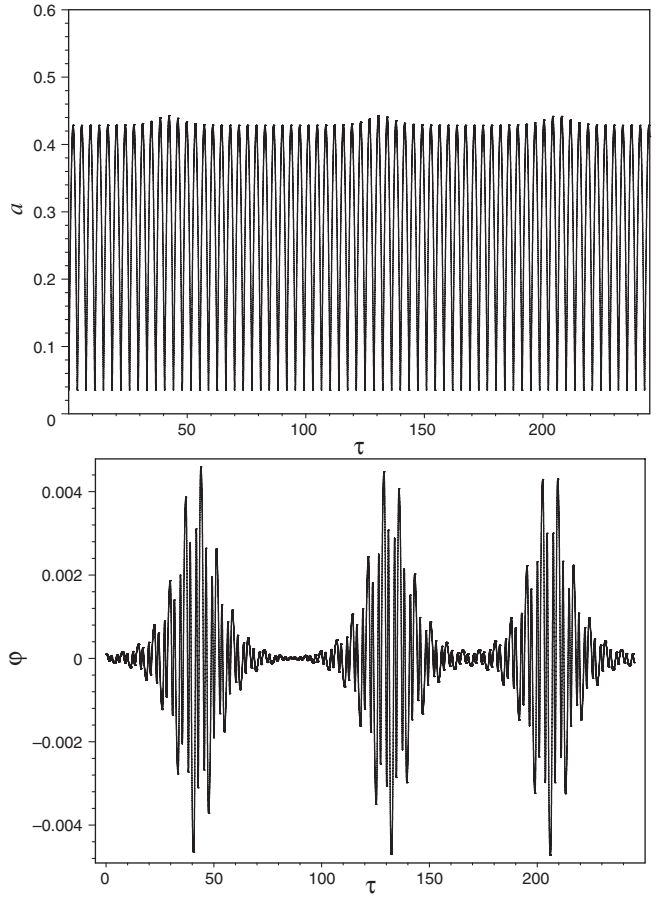

FIG. 8. Time signals for $m = 8.6$ and $|\sigma| = 350$, corresponding to the region (iii) near the right border of the $n = 3$ resonance window of Fig. 3. The motion is resonant and chaotic, but otherwise stable, with no exit to inflation.

The above substructure appears to be a feature of the whole resonance window, as we have checked for other values of $|\sigma|$ in the $n = 3$ window, as well as for other resonance windows. It is worth mentioning that in the case of pure dust the subdomain of disruptive resonances is a very thin sheet on the left border of the resonance window, while the larger portion of the window that allows for escape corresponds to long-time diffusion.

Finally, we should remark that—as concerning nonlinear resonance phenomena—the general picture is that bouncing oscillating braneworld models have a small restricted domain in their parameter space where inflation can be realized. Typically, variation of the parameters can shrink or stretch the resonance zones. However, the underlying pattern of resonance windows and their internal substructure is maintained as we have checked numerically. In this sense the pattern is said to be structurally stable.

VII. PURE SCALAR FIELD BOUNCING COSMOLOGIES: METASTABLE DYNAMICAL CONFINEMENT

We now proceed to examine the case when the model has no perfect fluid component. As we will see, even then the bulk-brane corrections allow for the presence of either perpetually oscillatory or metastable oscillatory models that emerge into an inflationary phase after a finite time. The dynamical equations in this case are given by Eq. (21), namely, the KG equation

$$\varphi'' + (1 + m^2 a^2)\varphi = 0,$$

plus the modified Eq. (19)

$$a'^2 + a^2 - \frac{\Lambda_4}{3} a^4 + \frac{1}{6a^4}\Delta^2(\varphi) - \frac{|\sigma|}{3}\Delta(\varphi) = 0, \quad (43)$$

where

$$\Delta(\varphi) = \tfrac{1}{2}[\varphi'^2 + (1 + m^2 a^2)\varphi^2]. \quad (44)$$

For the integrable case $m = 0$, we have that $\Delta_0 \equiv [\varphi'^2(\tau) + \varphi^2(\tau)]/2 \equiv [\varphi'^2(0) + \varphi^2(0)]/2$ is a constant of motion and Eq. (43) reduces then to

$$a'^2 + V(a) = \frac{|\sigma|}{3}\Delta_0, \qquad V(a) = a^2 - \frac{\Lambda_4}{3} a^4 + \frac{\Delta_0^2}{6a^4}, \quad (45)$$

so that the dynamics of the scale factor $a(\tau)$ is analogous to that of a radiation dominated bouncing braneworld universe with total energy content Δ_0 (cf. Eqs. (19) and (21) for $E_{\rm rad} \neq 0$, other E_i=0). Physical motion imposes the constraint $V(a_{\rm min}) \leq |\sigma|\Delta_0$, where $V(a_{\rm min})$ is the minimum of the potential (45), the inequality corresponding to oscillatory motion. A distinct feature of the phase space is that the infinite barrier avoiding the singularity as well as the constant of motion $|\sigma|\Delta_0$ are both built up with the nonzero initial amplitudes of the inflaton field. A portrait of

the phase space plane (a', a)—analogous to that in Fig. 2—may be constructed by varying $|\sigma|\Delta_0$. In the domain $V(a_{\min}) \leq |\sigma|\Delta_0 < V(a_{\max})$ the dynamics lies on tori that are the product of the periodic orbits in this phase plane times the circles $\varphi'^2 + \varphi^2 = 2\Delta_0$. The minimum configuration is a stable Einstein universe sourced by a massless inflaton. This stable Einstein universe is a limiting one-dimensional torus, being actually the product of the point $(a' = 0,\ a = a_{\min})$ times the circle defined by $\Delta_0 = V(a_{\min})/|\sigma|$. Contrary to the cases with a perfect fluid component, the Einstein universe is not a critical point of the dynamics. No invariant plane is present.

The compact phase space domain containing tori is analogously restricted by (34) with the obvious substitution of E_0 by Δ_0. We note that, for fixed σ and Λ_4, each of the integrable tori is generated by just one curve with initial conditions (φ'_0, φ_0). In this sense the energy surfaces $|\sigma|\Delta_0 = \text{const}$ contain just one curve.

An analogous portrait can be constructed for a single orbit with initial conditions (φ'_0, φ_0) by varying σ, characterizing thus universes with distinct gravitational strengths $G_N = |\sigma|/8\pi$. The corresponding tori yield qualitatively the same stable dynamics, about the stable Einstein universe sourced by a massless conformal inflaton with a minimal gravitational strength.

For the nonintegrable case, with m small (and $|\sigma|m^2\varphi(0)^2/6$ sufficiently smaller than 1, as we discuss below), the pattern is that of stable motion on KAM invariant tori or between two invariant KAM tori resulting from the integrable case. The stability of motion implies that all orbits are trapped between invariant tori and cannot escape to inflation, namely, inflation cannot be realized for these configurations. This is illustrated in Fig. 9 where we construct the Poincaré map with surface of section $a' = 0$ for fixed parameters $(\Lambda_4 = 1.5,\ |\sigma| = 500,\ m = 8.15)$. The innermost circle about the origin of the map is the section of the one-dimensional torus [namely, the periodic orbit in the plane (φ', φ)] corresponding to the stable Einstein universe. In this example the stable Einstein universe—sourced by a massive $(m = 8.15)$ conformal inflaton—is described by $a' = 0$, $a \simeq 0.00\,519\,690\,052)$ times the circle in the (φ', φ) plane generated, for instance, from the initial conditions $(\varphi'(0) = 0,\ \varphi \simeq 0.000\,696\,503\,226)$ with associated energy constant $\Delta_0 \simeq 0.2\,429\,935 \times 10^{-6}$. Below this scalar field energy no oscillatory motion is found, resulting in the void (no physical motion) about the origin of the map bounded by the above described innermost circle. The pattern of KAM tori sections, with eventual bifurcated secondary islands, extends up to initial conditions $a' = 0$, $\varphi' = 0$, and $\varphi_0 \simeq 0.01\,105$, where approximately the last confining KAM torus lies. In this region of trapped orbits we may note, for instance, 8 secondary islands (the far right centered about $\varphi_0 = 0.01\,079$) connected to a $8/5$ bifurcation. The outside region, denoted the stochastic sea in border of the main

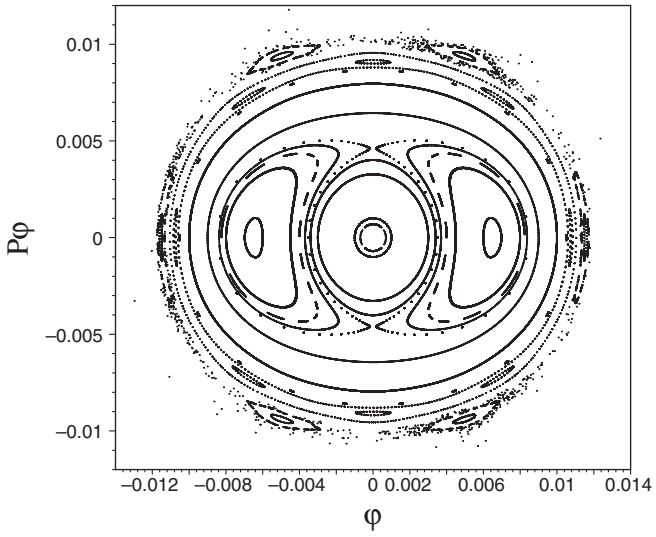

FIG. 9. Poincaré map with surface of section $a' = 0$ for pure scalar filed cosmologies, with $|\sigma| = 500$ and $m = 8.15$. The innermost circle about the origin is a one-dimensional torus corresponding to a stable Einstein universe sourced by a scalar field. The domain inside this circle is unphysical. The last KAM torus shown has initial conditions $(\varphi'_0 = 0,\ \varphi_0 \simeq 0.01\,105)$. Escape to inflation may occur in the outer border (for $\varphi_0 > 0.01\,105$) with oscillatory motion due to partial confinement of orbits.

KAM island, corresponds to the domain of initial conditions where inflation can be realized in pure scalar field sourced braneworld cosmologies. In this stochastic sea we may have either a rapid escape to inflation (for $\varphi_0 = 0.0118$ with $\tau \simeq 210$, or for $\varphi_0 = 0.01\,125$ with $\tau \simeq 500$, for instance) or a diffusion with escape, for instance about the border of the two sets of 3 secondary islands connected to a $3/2$ bifurcation (for $\varphi_0 = \pm 0.011\,305$ with $\tau \simeq 1690$). For larger initial conditions, namely $\varphi_0 \gtrsim 0.01\,234$, no bifurcated islands are found in the stochastic sea but finite time oscillations are still found due to a mechanism of dynamical partial confinement, connected to values of the parameter

$$\varsigma \equiv |\sigma|m^2\varphi(0)^2/6, \tag{46}$$

sufficiently close to 1, as we describe in the following.

Let us recall that the potential $V(a)$ in (45) presents a well (with possible oscillatory motion) for properly bounded values of Δ_0 restricted by (34). Furthermore, $V(a) - |\sigma|\Delta_0/3 = 0$ must have three real positive roots such that oscillatory motion is present. However, the restriction (34) was derived for the integrable case and for the spatial curvature parameter rescaled to $k = 1$. Actually the presence of the physical well is due to the balance between the spatial curvature term and the infinite barrier term originated from the bulk-brane correction, more specifically, the balance between the values of the parameters k and Δ_0. It is not difficult to see that, in the integrable case,

the decrease (increase) of k with Δ_0 fixed as well as the increase (decrease) of Δ_0 for k fixed, may destroy (or create) a well. Now for the nonintegrable case ($m \neq 0$) a careful examination of the integral constraint (43) shows that the term proportional to m^2 in the RHS will contribute to correct the curvature term to an effective spatial curvature ($k_{\rm eff} \simeq 1 - \varsigma$) at the initial times. For the parameter configuration of Fig. 9 numerical evaluations show that the above effects will be crucial for the dynamics of the scale factor $a(\tau)$ when $k_{\rm eff} \lesssim 0.157$, that corresponds to $\varphi_0 \gtrsim 0.01\,234$. In this instance, two possibilities arise: (i) for $0.01\,234 \lesssim \varphi_0 < 0.1334$, $\varphi_0' = 0$, the function

$$\mathcal{P}(a) \equiv a^2 - \frac{\Lambda_4}{3}a^4 + \frac{1}{6a^4}\Delta^2(\varphi_0) - \frac{|\sigma|}{3}\Delta(\varphi_0), \quad (47)$$

[cf. (43)] has two extrema (one maximum and one minimum) but $\mathcal{P}(a) = 0$ has only one real positive root a_0, meaning that the value of the relative maximum of $\mathcal{P}(a)$ is smaller than zero. The orbit evolved from this initial condition would in principle be expected to escape without bounce. However, due to the increase of the effective time-dependent spatial curvature $k_{\rm eff} \simeq 1 - |\sigma| m^2 \varphi(\tau)^2/6$, the relative maximum of $\mathcal{P}(a)$ is raised above zero at a later time so that the orbit bounces back. This is illustrated in Fig. 10(a) where we plot $\mathcal{P}(a)$ for the initial time with ($\varphi_0' = 0$, $\varphi_0 = 0.0126$), which has the only real root $a_0 \simeq 0.016\,955\,927\,198$ (continuous curve), and for the time of the first bounce of the orbit generated from these initial conditions (dashed curve). The first bounce corresponds to the point ($\varphi_0' \simeq -0.0\,144\,932$, $\varphi_0 \simeq -0.00\,419\,929$) with $k_{\rm eff} \sim 0.9$. We note that the dashed curve represents a dynamical potential with its maximum above zero, allowing for the bounce. The adjustment of this effect with the period of the massive scalar field allows for a series of bounces of the orbit before it finally escapes, as shown in Fig. 10(b). (ii) For $\varphi_0 \gtrsim 0.1334$ $\mathcal{P}(a)$ has no extremum but due to the effective time-dependent curvature two extrema are dynamically created, with the relative maximum above zero, so that the orbit undergoes bounces in a relatively smaller number than in case (i) before escaping. It is worth mentioning that this effect may be present for $\varphi_0 < 0.01\,234$, provided we properly increase the parameters m and/or $|\sigma|$ to turn ς sufficiently small.

Finally, we should remark that the dynamics of pure scalar field brane cosmologies is not connected to a parametric resonance pattern. The features of initial condition domains that realize inflation in this case are similar to the ones for the domain of parametric stability (compare the Poincaré maps in Fig. 4 (bottom) and Fig. 9), as the configurations that realize inflation are the ones at the border of the primary KAM islands, corresponding to large values of φ.

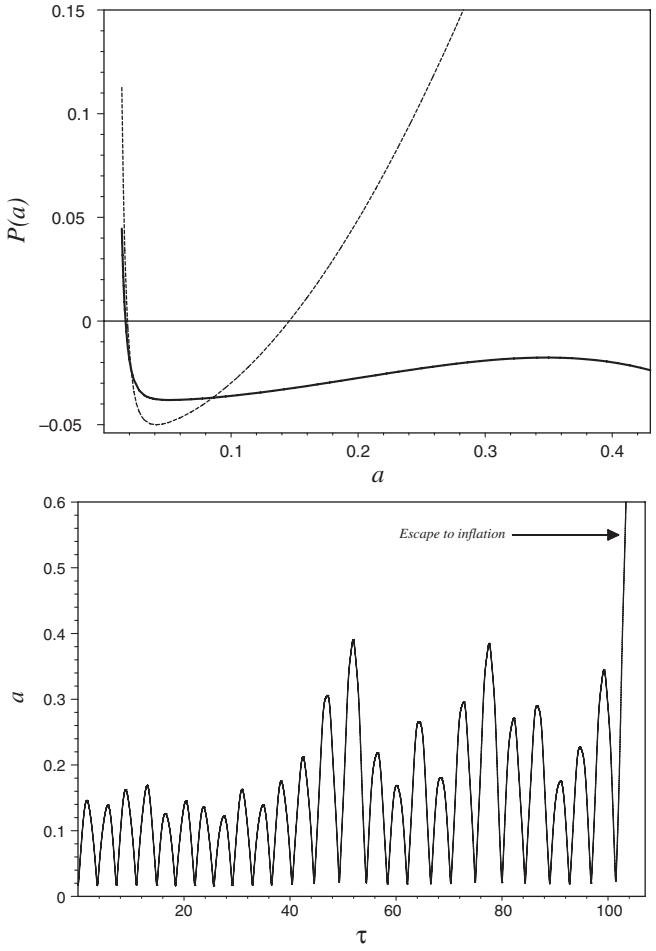

FIG. 10. Plot of the function $\mathcal{P}(a)$ for the initial time (continuous curve) and the time of the first bounce (dashed curve). The occurrence of the bounce is due to the dynamical raising of the potential as a consequence of the increase of the effective spatial curvature $k_{\rm eff}(\tau)$ as φ decreases. The first bounce occurs when $k_{\rm eff} \sim 0.9$. A sequence of this process produces the oscillatory behavior shown below.

VIII. MOTION ABOUT THE SADDLE-CENTER: HOMOCLINIC CHAOS AND THE CHAOTIC EXIT TO INFLATION

The saddle-center critical P_1 induces, in the phase space of the models, the topology of stable and unstable homoclinic cylinders, which emanate from unstable periodic orbits that exist in their neighborhood. This structure was examined in some detail in [19] and is briefly discussed here for completeness. The nonintegrability of the dynamics induces the breaking and crossing of the homoclinic cylinders leading to a chaotic exit to inflation as we proceed to show in this section, where for simplicity we restrict ourselves to two perfect fluid components (dust and radiation only) as in Sec. IV.

Our starting point is a fundamental property of saddle-centers given by Moser's theorem [20]. Moser's result states that it is always possible to find a set of canonical

variables such that in a small neighborhood of a saddle-center the energy integral of motion (19) is separable into rotational and hyperbolic motion pieces. The variables $(a, p_a, \varphi, p_\varphi)$ of our system are already of the Moser type and, in a linear neighborhood of P_1, we have the separable rotational motion energy piece $E_{(\varphi)}$ and the hyperbolic motion energy piece $E_{(a)}$ as expressed in (28). We recall that in this case $V''(a_{\rm crit}) < 0$. In this approximation, we note that the scale factor $a(\tau)$ has pure hyperbolic motion and is completely decoupled from the pure rotational motion of the inflaton fluctuation φ. Let us consider the possible motions in this neighborhood. In the case of $E_a = 0$ and $p_a = 0 = (a - a_{\rm crit})$, the motion corresponds to unstable periodic orbits $\mathcal{T}_{|\sigma|E_{\rm rad}}$ in the plane (φ, p_φ). Such orbits depend continuously on the parameter $|\sigma|E_{\rm rad}$. For $E_a = 0$ there is still the possibility $p_a = \pm\sqrt{6|V''(a_{\rm crit})|}(a - a_{\rm crit})$, which defines the linear stable V_S and unstable V_U one-dimensional manifolds. The direct product of the periodic orbit $\mathcal{T}_{|\sigma|E_{\rm rad}}$ with V_S and V_U generates, in the linear neighborhood of the saddle-center, the structure of pairs of stable $(\mathcal{T}_{|\sigma|E_{\rm rad}} \times V_S)$ and unstable $(\mathcal{T}_{|\sigma|E_{\rm rad}} \times V_U)$ two-dimensional cylinders. We note that for $E_{\rm crit} \approx |\sigma|E_{\rm rad}$ the manifolds V_S and V_U are tangent at P_1 to the separatrices $\mathcal{S}$ of the invariant plane containing the saddle-center; hence a pair of cylinders (one stable and one unstable) emanates from the neighborhood of P_1 toward $a \sim 0$, while another pair emanates towards the two de Sitter attractors at infinity (cf. Figure 1). Orbits on the cylinders coalesce into the periodic orbit $\mathcal{T}_{|\sigma|E_{\rm rad}}$ asymptotically, the orbits being contained in the same energy surface $|\sigma|E_{\rm rad}$ as that of the periodic orbit; these orbits are denoted homoclinic to the periodic orbit $\mathcal{T}_{|\sigma|E_{\rm rad}}$ or simply homoclinic orbits. Noticing that in general $E_{(a)} - |\sigma|E_{(\varphi)} + E_{\rm crit} - |\sigma|E_{\rm rad} \sim 0$ [cf. (27) and (28)] and that E_φ is strictly positive we must have $E_{\rm crit} - |\sigma|E_{\rm rad} > 0$; hence, only energy surfaces satisfying this condition contain homoclinic cylinders.

The nonlinear extension of the plane of rotational motion (when $\mathcal{O}(3)$ terms in (27) are taken into account) is a two-dimensional manifold, the *center manifold* of unstable periodic orbits of the system parametrized with the energy $|\sigma|E_{\rm rad}$. The intersection of the center manifold with the energy surface $|\sigma|E_{\rm rad}$ is a periodic orbit $\mathcal{T}_{|\sigma|E_{\rm rad}}$ from which two pairs of cylinders emanate, as in the linear case previously described. It can be shown that in general the nonlinear extension of the center manifold folds, so that the unstable periodic orbits are no longer contained in the plane (φ, p_φ). Now the extension of the cylinders away from the periodic orbits depends crucially on the integrability or nonintegrability of the system.

In the integrable case $(m = 0)$ the homoclinic cylinders are the topological product of the separatrices $\mathcal{S}$ times the periodic orbit with energy $\mathcal{E}^0_\varphi$. We are basically interested in the pair of cylinders (one stable and one unstable) that emerge from the periodic orbit toward decreasing values of a, namely, in Region I. It is not difficult to see that, in the integrable case, the unstable cylinder coalesces smoothly into the stable one. However, when the nonintegrability is switched on (namely, $m \neq 0$), the smooth continuation of the unstable cylinder into the stable one breaks, inducing the transversal crossing of them. The points of intersection define homoclinic orbits, which emerge from the periodic orbit along the unstable cylinder and return to it along the stable one, in an infinite time. Typically if the two-dimensional cylinders intersect transversally once, they will intersect each other an infinite number of times, producing an infinite set of homoclinic orbits that are bi-asymptotic to the unstable periodic orbit of the center manifold. This infinite set of homoclinic orbits is denoted the intersection manifold. The dynamics near homoclinic orbits is very complex, associated with the presence of the well-known horseshoe structures (cf. [14,21] and references therein), with the homoclinic intersection manifold giving origin to the homoclinic tangle, which is a signature of chaos in the model.

This manifestation of homoclinic chaos is illustrated in Fig. 11 where the fractality of the initial conditions basin boundaries, connected to the code recollapse/escape into inflation is shown. We select the initial condition set whose projection on (φ, p_φ) is a square of characteristic length $R \simeq 10^{-3}$, constructed about the point $(a = 0.15,\ p_a = 3.114\,327\,925\,239\,397,\ \varphi = 0,\ p_\varphi = 0)$ close [22] to the separatrix $\mathcal{S}$ reaching P_1, containing $N = 160\,000$ initial conditions. These points obviously satisfy the constraint Eq. (29), with $E_{\rm dust} = E_{\rm rad} = 10^{-3}$ and $|\sigma| = 762$, such that $|\sigma|E_{\rm rad}$ is slightly below $E_{\rm crit} \equiv V_{\rm max}$. We note that these sets correspond to initial conditions for expanding universes that visit a neighborhood of the saddle-center P_1 before either to recollapse or to escape into inflation. The points of the square are color-coded according to their

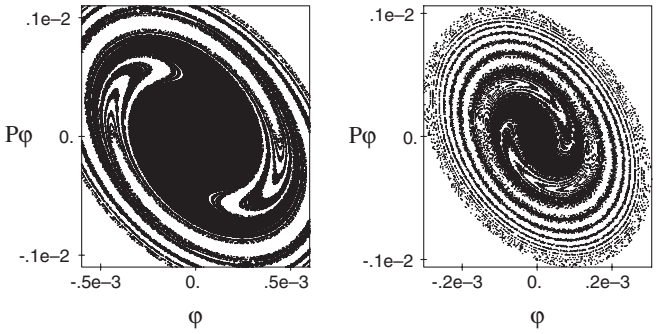

FIG. 11. Fractal basin boundaries, in the plane (φ, p_φ), of initial condition sets for initially expanding universes that visit a small neighborhood of the saddle-center before either recollapsing or escaping to inflation, in the case $E_0 = E_1 = 10^{-3}$. Black points correspond to orbits that recollapse to the domain $a \simeq 0$ and white points correspond to orbits that escape to inflation, for a time $\tau = 4000$, and $m = 6$ (left) and $m = 18$ (right).

asymptotic behavior for a time $\tau = 4000$—white corresponding to escape into inflation and black corresponding to recollapse to the neighborhood $a \simeq 0$—resulting in the plots of Fig. 11 for $m = 6$ and $m = 18$. We notice that as we increase m, namely, as the system becomes more nonintegrable, the dominance of escape into inflation and fractality of the boundaries increase, characterizing a chaotic exit to inflation. The dynamics involves no amplification of the inflaton field (namely, φ and/or p_φ), as opposed to the metastable nonlinear resonance regime before escape to inflation, described in Secs. V and VI.

The entanglement and infinite transversal crossings of the stable with the unstable homoclinic cylinders engender a further mechanism in the chaotic exit to inflation, which we denote as *draining of initial condition basins*. Let us remark on the fact that the surface of the cylinders constitute a boundary for the general flow. If we start, for instance, with a set of initial conditions corresponding to initially expanding universes, two distinct flows will be associated with these initial conditions depending on whether they are contained inside or outside the stable cylinder. The flow corresponding to initial conditions inside the stable cylinder will reach a neighborhood of the saddle-center P_1 (with $E_a < 0$) and will return toward the neighborhood of $a \simeq 0$ inside the unstable cylinder, while the flow of orbits associated with initial conditions that are outside the cylinder will reach the neighborhood of P_1 and escape toward the de Sitter attractor along the exterior of the unstable cylinder of the second pair. Now consider the first transversal intersection of the cylinders: a part of the orbits inside the unstable cylinder will enter the interior of the stable cylinder and the flow will proceed inside the stable cylinder toward the neighborhood of P_1, from where it will reenter the unstable tube and proceeds toward the region $a \simeq 0$ and by a new intersection a part of these orbits will again enter the stable tube and proceeds back toward the neighborhood of P_1 and so on. The portion of orbits that in this subsequent intersection remained outside the stable cylinder will also proceed along it toward P_1 and will escape to inflation. As the motion proceeds, the successive infinite intersections of the cylinders drain the basin of initial conditions from *black* to *white* as τ increases, as illustrated in Fig. 12, where we start from the initial condition set of Fig. 11 for $m = 6$, color coded at $\tau = 4000$ (in the present Figures we used $N = 40,000$ initial conditions only). The only orbits remaining in an infinite recurrence of the motion are the homoclinic orbits, which constitute the homoclinic intersection manifold, and the infinite countable set of periodic orbits with arbitrarily long periods in the neighborhood of each homoclinic orbit. These orbits constitute a Cantor set that is a topological characterization of chaos in the model [14].

Finally, in Fig. 13 we exhibit two initial condition sets for $m = 6$, color coded at $\tau = 4000$, in the cases of pure dust (left) and pure radiation (right), both with $N = 160\,000$ points. For the radiation case the initial set was

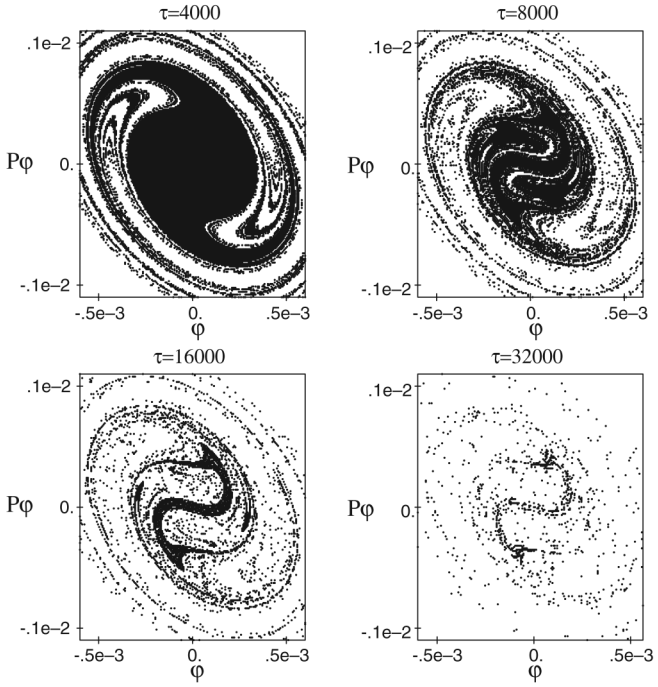

FIG. 12. Illustration of the process of draining (in time) the initial condition basin of trapped orbits (black) in favor of escaping orbits (white), for $m = 6$. The initial condition set taken about the separatrix is the same as in Fig. 11. The figures show the almost complete exit to inflation (up to a Cantor set of orbits) in a long-time term.

constructed about the point $(a_0 = 0.15,\ p_{a0} = 4.144\,304\,603\,687\,830,\ \varphi_0 = 0 = p_{\varphi 0})$, sufficiently close to the separatrix, with $|\sigma| = 1499$ and $E_{\rm rad} = 10^{-3}$. For dust the initial set was constructed about the point $(a = 0.15,\ p_a = 1.460\,426\,592\,928\,701,\ \varphi = 0 = p_\varphi)$, also sufficiently close [22] to the separatrix, with $|\sigma| = 1630$ and $E_{\rm dust} = 10^{-3}$, both sets also with characteristic length $R \simeq 10^{-3}$. Thus, the mechanism of chaotic exit to inflation is enhanced in the case of dust plus radiation (see Fig. 11), in

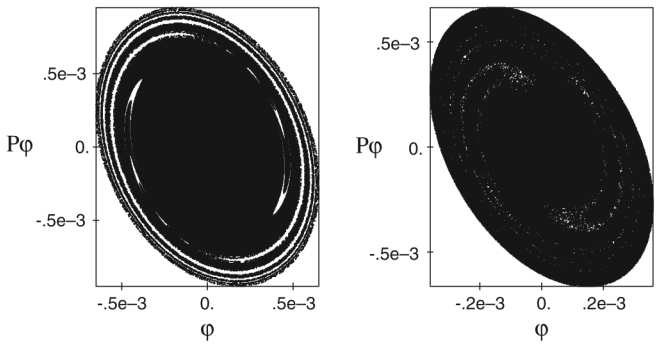

FIG. 13. Fractal basin boundaries in the plane (φ, p_φ) for pure dust (left) and pure radiation (right), for $m = 6$ and color coded at $\tau = 4000$. The fractalization of the boundaries appears less effective in both cases than in the case of radiation plus dust of Fig. 11 (left).

comparison with the case of pure dust or pure radiation components.

The chaotic exit to inflation examined in the present section is not a feature of bouncing inflationary cosmologies only. In fact, a similar pattern for fractal initial conditions basin boundaries connected to the escape to inflation was observed and discussed by Cornish and Levin [23] in the context of singular closed FRW cosmologies sourced with several conformally and/or minimally coupled scalar fields. An extensive analysis showed that the pattern is typical for the nonintegrable cases of the models, and a quantitative measure of the fractality was made by evaluating the box-counting dimension of the boundaries. The effect of *draining of initial conditions* from recollapse to escape as time increases, observed in our models, is not seen there due to the absence of bounces that avoid the singularity and allow for a long-time recurrence. The Cantor set resulting from this effect as $\tau \to \infty$ corresponds to the strange repeller structure already appearing in their dynamics.

IX. CONCLUSIONS AND FINAL DISCUSSIONS

In the present paper we construct nonsingular cosmological scenarios, in the realm of string inspired braneworld models, which are past eternal, oscillating, and may emerge into an inflationary phase due to nonlinear resonance mechanisms. We consider a closed FRW metric on the four-dimensional braneworld embedded in a five-dimensional conformally flat bulk. Local bulk effects on the four-dimensional FRW braneworld introduce corrections in Friedmann's equations that allow to implement nonsingular bounces in the scale factor of the models. This is the case of a timelike extra dimension, when the corrections result in a repulsive force that avoids the singularity and provide a concrete model for bounces in the early phase of the universe. The matter content of the model, confined to the FRW brane, consists of noninteracting perfect fluids with equation of state $\rho_i = \alpha_i p_i$, with $-1/3 < \alpha_i \leq 1$, plus a massive conformally coupled scalar field. In the FRW brane the energy density of the fluids are $\rho_i = E_i/a^{3(1+\alpha_i)}$, where the constant of motion E_i is proportional to the total energy of the respective fluid. The corrections in Friedmann's equations resulting from the bulk-brane interaction are quadratic in the energy-momentum tensor of the matter fields on the brane. The resulting dynamics is nonintegrable and chaotic if the mass of the inflaton $m \neq 0$, allowing for metastable configurations that realize inflation due to parametric nonlinear of KAM tori present in the phase space of the model.

Our analysis is restricted to dynamical configurations in which the dynamics of the scale factor is initially bounded in a potential well arising in the gravitational sector (a, p_a) due to the effective cosmological constant, the positive spatial curvature of the brane, and the bulk-brane corrections (connected with the perfect fluid components) that act as infinite potential barrier and is responsible for the avoidance of the singularity $a = 0$. These configurations have the theoretical advantage over one-single bounce models in that they avoid the problem of initial conditions for the Universe at past infinity. Furthermore, they are past eternal, oscillating about a stable Einstein universe configuration, that has no classical analogue and is favored by maximum entropy considerations [15]. The skeleton of the phase space dynamics is analyzed through its basic structures as critical points (stable and unstable Einstein universe), invariant plane, separatrices and de Sitter attractors at infinity, as well as the foliation by KAM tori of the phase space in the nonlinear neighborhood of the stable Einstein universe. The stable Einstein universe is a critical point of the dynamics when sourced by perfect fluids, or a limiting one-dimensional torus (namely, the topological product of a point times a minimal periodic orbit in the scalar field sector) when sourced by a scalar field in pure scalar field cosmologies.

For particular domains of the parameter space $(\Lambda_4, \sigma, E_i, m)$ of the model, denoted windows of resonance, these oscillatory bounded configurations turn metastable due to nonlinear parametric resonance phenomena, allowing the emergence of the Universe into an inflationary phase. For numerical/analytical simplicity, we made an extensive examination of parametric resonance phenomena in braneworld models restricted to a dark energy component and radiation (i = dust, rad), plus the massive inflaton field and a dark energy component described by the effective cosmological constant in the brane. We constructed the resonant chart for the case of $E_{\rm dust} = E_{\rm rad} = 10^{-3}$, shown in Fig. 3, where the windows of resonance are the gray sheets. The white regions correspond to stable motion. When the system is driven toward a resonance window, nonlinear resonance of KAM tori takes place resulting in a complex dynamics. KAM tori that trapped the orbits are disrupted, and the initially bounded, oscillatory orbits of the system may escape to the deSitter attractor at infinity realizing inflation. We illustrated this behavior by Poincaré maps in the plane (φ', φ), the origin of which corresponds to a stable or unstable periodic orbit whether, respectively, the system is in a stable region or a resonance window of the resonance chart.

Each resonance window is characterized by an integer $n \geq 2$, and its main feature is the bifurcation of the stable periodic orbit at the origin ($\varphi = 0$, $p_\varphi = 0$) into an unstable periodic orbit accompanied by one or two characteristic stable periodic orbits whether respectively n is odd or even. As the initial conditions of the expectation values φ are assumed to be small, being taken near the invariant plane $\varphi = 0$, $p_\varphi = 0$, it follows that the parametric domains of resonance are the ones that allow for inflation in the system. In this sense, since inflation is a sound paradigm for cosmology strongly sustained by observations,

and if our present Universe is actually a braneworld, then the values of the cosmological parameters must be constrained to the resonance windows—with the braneworld inflated from initial conditions connected to a particular resonance. In particular, for fixed m and E_i, the brane tension σ that regulates the strength of the effective Newton's constant in the brane will be restricted to small sheets depending on the integer $n \geq 2$ (cf. Figure 3). Therefore, the larger the order of the resonance the stronger the gravitational coupling strength in the in the respective brane inflated due to a specific resonance. In this instance, we observe a *quantization* of the brane tension and consequently of the effective Newton's constant.

The volume of the resonance windows are small as compared to the whole volume of the parameter space. The size of these four-dimensional volumes depends strongly on the fluid content of the model. In Fig. 5 we exhibited the windows corresponding to the $n = 3$ resonance for pure dust, pure radiation, and dust plus radiation in equal amounts ($E_{\mathrm{rad}} = E_{\mathrm{dust}}$). The case in which the perfect fluid component is dust only presents resonance windows with a reduced volume compared with pure radiation windows, analogously to the substructure of disruptive resonances in each window. This suggests that if we demand that our preinflationary models contain a component of dark matter in the form of dust this amount should be properly bounded in order that the model could realize inflation.

Three distinct dynamical patterns are set up by the resonance, according to substructures in the resonance windows in models with $E_{\mathrm{dust}} \leq E_{\mathrm{rad}}$ as observed by a detailed numerical examination. If the initial conditions correspond to configurations in the left border of the resonance windows we have short time disruption of the initially bounded orbit with a rapid escape to inflation. On the other hand, if the initial conditions correspond to configurations in an intermediate threshold region of the window the orbit undergoes a long-time diffusion in the stochastic sea surrounding the two secondary KAM stability islands, with posterior escape to inflation. Beyond the threshold region, near the right border of the window, the orbit undergoes diffusion through large regions of phase space but remains bounded for times larger than $\tau = 100\,000$. This latter region of the resonance window should then be excluded as physically not admissible since they correspond to configurations that do not realize inflation.

We also examined cosmological scenarios with a pure scalar field. Because of the absence of any perfect fluid component, the bulk-brane correction term that allows the dynamics to avoid the singularity is crucially dependent on the nonzero initial amplitude of inflaton through the conserved energy $\Delta_0 = (\varphi'(0)^2 + \varphi(0)^2)/2$. Contrary to the cases with a perfect fluid component, the stable Einstein universe is not a critical point but a limiting one-dimensional tori, sourced by a scalar field. For a fixed σ each energy surface contains just one torus generated by a single orbit. The escape to inflation in the nonintegrable case is not associated to a parametric resonance pattern and occurs just for configurations of the scalar field with large initial conditions, in the small stochastic sea on the border of the main KAM island shown in Fig. 9. In this outer border we observe a mechanism of dynamical partial confinement of orbits, leading to finite time oscillations before escape to inflation. Also, contrary to models with a perfect fluid component, the structure of the bouncing dynamics is extremely sensitive to the initial amplitude and to the mass of the scalar field, and the presence of dynamical potential barriers allowing for bounces in the scale factor appears as a new feature of the dynamics.

In Sec. VIII we examined the chaotic exit to inflation for initial condition sets (corresponding to initially expanding universes) taken in a small neighborhood about the stable separatix $\mathcal{S}$. These sets are shown to have fractal basin boundaries connected to the code recollapse/escape to inflation leading to a chaotic exit to inflation. The fractality of the initial condition sets increases with m, namely, with the nonintegrability and their escape to inflation takes place smoothly involving no strong amplification of the inflaton field, as opposed to the metastable nonlinear resonance regime immediately before the exit to inflation, as discussed in Secs. V and VI. We also observe the phenomenon of draining of these initial condition basins from recollapse to escape behavior, as time increases. For $\tau \rightarrow \infty$ only the homoclinic intersection manifold remains in recurrent oscillatory motion. The homoclinic chaotic exit to inflation appears to be enhanced in the case of dust plus radiation, relative to the cases with pure dust or pure radiation components, contrary to what occurs in the parametric resonance escape to inflation. We have not examined the possibility of chaotic escape to inflation in pure scalar field cosmologies.

Typically, variation of the parameters can shrink or stretch the resonance zones. However, the underlying pattern of resonance windows is maintained as we have checked numerically. In this sense the pattern is said to be structurally stable. Finally, if our actual Universe is a brane inflated by a parametric resonance mechanism triggered by the inflaton, some observable cosmological parameters (e.g. Newton's gravitational constant on the brane and the mass of the inflaton) should then have a signature of the particular resonance from which the brane inflated and consequently of the particular value of the parameters (σ, m, E_{dust}, E_{rad}) that were favored in the early dynamical regime of the Universe.

ACKNOWLEDGMENTS

The authors acknowledge partial financial support from CNPQ-MCT/Brasil. Several of the figures were generated using the DYNAMICS SOLVER packet [24].

[1] M. Bojowald (Loop Quantum Cosmology Collaboration), Living Rev. Relativity **8**, 11 (2002), http://relativity.livingreviews.org/Articles/lrr-2005/11; M. Bojowald and R. Tavakol, arXiv:gr-qc/08024274.
[2] K. R. Dienes, Phys. Rep. **287**, 447 (1997); M. Kaku, *Strings, Conformal Fields, and M-theory* (Springer-Verlag, New York, 2000); C. Rovelli, Living Rev. Relativity **1**, 1 (1998).
[3] L. Randall and R. Sundrum, Phys. Rev. Lett. **83**, 4690 (1999); **83**, 3370 (1999).
[4] T. Shiromizu, K. Maeda, and M. Sasaki, Phys. Rev. D **62**, 024012 (2000).
[5] R. Maartens, Phys. Rev. D **62**, 084023 (2000); R. Maartens, Living Rev. Relativity **7**, 7 (2004).
[6] Y. V. Shtanov, arXiv:hep-th/0005193; Phys. Lett. B **541**, 177 (2002); Yu. Shtanov and V. Sahni, Phys. Lett. B **557**, 1 (2003).
[7] H. P. Oliveira, I. Damião Soares, and E. V. Tonini, J. Cosmol. Astropart. Phys. 02 (2006) 015; R. F. Aranha, H. P. Oliveira, I. Damião Soares , and E. V. Tonini, J. Cosmol. Astropart. Phys., 10, (2007) 08.
[8] R. M. Wald, *General Relativity* (University of Chicago Press, Chicago, 1984).
[9] W. Israel, Nuovo Cimento B **44**, 1 (1966).
[10] V. Faraoni, Phys. Rev. D **62**, 023504 (2000).
[11] N. D. Birrel and P. C. Davies, *Quantum Fields in Curved Spacetimes* (Cambridge University Press, Cambridge, 1982).
[12] L. H. Ford, arXiv:gr-qc/0514096.
[13] A. Mielke, P. Holmes, and O. O'Reilly, J. Dyn. Differ. Equ. **4**, 95 (1992); W. M. Vieira and A. M. Ozorio de Almeida, Physica D (Amsterdam) **90**, 9 (1996).
[14] J. Guckenheimer and P. Holmes, *Dynamical Systems and Bifurcations of Vector Fields* (Springer-Verlag, New York, 1983).
[15] G. W. Gibbons, Nucl. Phys. **B292**, 784 (1987); **B310**, 636 (1988).
[16] M. Abramowitz and I. Stegun, *Handbook of Mathematical Functions*, NBS Applied Math. Series Vol. 55 (National Bureau of Standards, Washington, DC, 1964).
[17] A. N. Kolmogorov, in *Stochastic Behaviour in Classical and in Quantum Hamiltonian Systems*, edited by G. Casati and J. Ford, Lecture Notes in Physics Vol. 93 (Springer-Verlag, Berlin, 1979); V. I. Arnold, Russ. Math. Surv. **18**, 9 (1963); J. Moser, Nachr. Akad. Wiss. Gött., Math.-Phys. Kl. 2a **2**, 1 (1962);
[18] The correction of $\nu_\varphi = \frac{1}{2\pi}$ into $\tilde{\nu}_\varphi$ in Eq. (38) is obtained by using the exact equation $\ddot{\varphi} + (1 + m^2 a^2(\tau))\varphi = 0$, substituting in it the solution $a_0(\tau)$ of the associated integrable case and extracting the dominant correction. For a distinct ratio of $E_{\rm rad}$ and $E_{\rm dust}$ the factor 0.9 is changed according to the approximate medium point of the oscillations of $a_0(\tau)$. These approximations are very efficient to localize the resonances, as shown in Fig. 3.
[19] G. A. Monerat, H. P. Oliveira, and I. Damião Soares, Phys. Rev. D **58**, 063504 (1998).
[20] J. Moser, Commun. Pure Appl. Math. **11**, 257 (1958).
[21] S. Wiggins, *Global Bifurcations and Chaos* (Springer-Verlag, Berlin, 1988); J. K. Moser, *Stable and Random Motions in Dynamical Systems* (Princeton University Press, Princeton, New Jersey, 1973); A. M. Ozorio de Almeida, *Hamiltonian Systems, Chaos and Quantization* (Cambridge University Press, Cambridge, England, 1993).
[22] The minimal distance from this point to the separatrix, in the Euclidean sense, is $\delta \simeq 10^{-3}$.
[23] N. J. Cornish and J. J. Levin, Phys. Rev. D **53**, 3022 (1996).
[24] Juan M. Aguirregabiria, Dynamics Solver, http://tp.lc.ehu.es/jma.html.